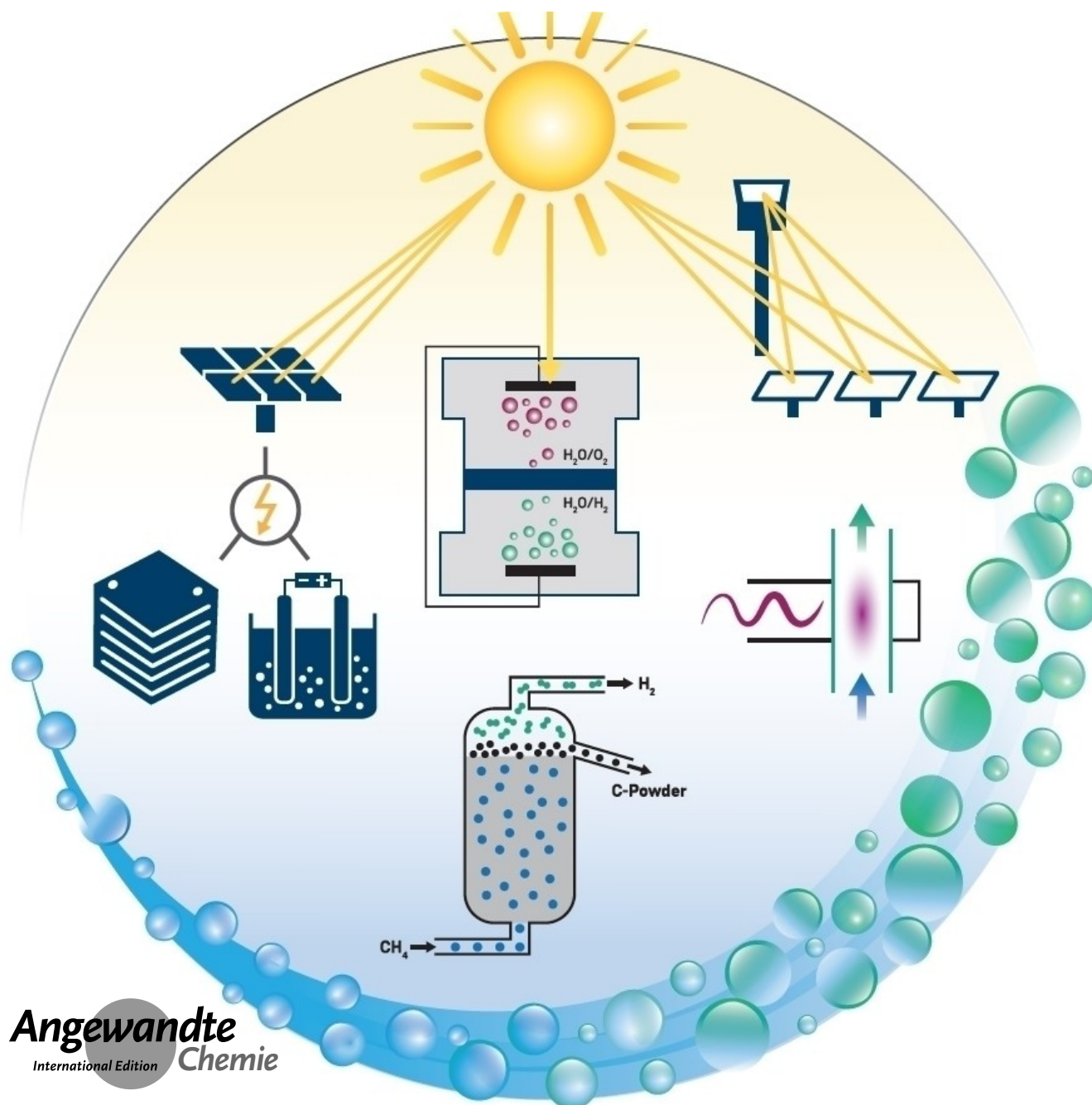


## Solar Hydrogen

# Technological Pathways to Produce Compressed and Highly Pure Hydrogen from Solar Power

Mariya E. Ivanova,\* Ralf Peters, Martin Müller, Stefan Haas, Martin Florian Seidler, Gerd Mutschke, Kerstin Eckert, Philipp Röse,\* Sonya Calnan, Rory Bagacki, Rutger Schlatmann, Cedric Grosselindemann, Laura-Alena Schäfer, Norbert H. Menzler, André Weber, Roel van de Krol, Feng Liang, Fatwa F. Abdi,\* Stefan Brendelberger,\* Nicole Neumann, Johannes Grobbel, Martin Roeb, Christian Sattler, Ines Duran,\* Benjamin Dietrich, M. E. Christoph Hofberger, Leonid Stoppel, Neele Uhlenbruck, Thomas Wetzler, David Rauner, Ante Hecimovic, Ursel Fantz,\* Nadiia Kulyk, Jens Harting,\* and Olivier Guillon



**Abstract:** Hydrogen (H<sub>2</sub>) produced from renewables will have a growing impact on the global energy dynamics towards sustainable and carbon-neutral standards. The share of green H<sub>2</sub> is still too low to meet the net-zero target, while the demand for high-quality hydrogen continues to rise. These factors amplify the need for economically viable H<sub>2</sub> generation technologies. The present article aims at evaluating the existing technologies for high-quality H<sub>2</sub> production based on solar energy. Technologies such as water electrolysis, photoelectrochemical and solar thermochemical water splitting, liquid metal reactors and plasma conversion utilize solar power directly or indirectly (as carbon-neutral electrons) and are reviewed from the perspective of their current development level, technical limitations and future potential.

## 1. Introduction

The production of green H<sub>2</sub> powered with renewable energy sources (solar, wind, hydro) is an important step towards a carbon-neutral future. The anticipated energy transition will reflect all areas, including a phase-out of fossils and “low carbon” hydrogen as short-to-medium-term bridging technologies. In this new era, H<sub>2</sub> will play a key role in the energy generation and storage. In line with the European Green Deal, the ambitious decarbonization targets will

prioritize the strengthening of sustainable and efficient H<sub>2</sub> production and storage and its secure distribution and transportation to various end users, including heat and power generation, and the overall supply chain. “H<sub>2</sub> valleys” as regional H<sub>2</sub> ecosystems will be paving the road to the global sustainable H<sub>2</sub> economy. Finally, the share of H<sub>2</sub> in Europe’s energy mix is projected to grow to 13–14 % by 2050 with more than 500 Mt H<sub>2</sub> per year produced, according to Hydrogen Council.<sup>[1]</sup> Therefore, the demand

[\*] Dr.-Ing. M. E. Ivanova, M.Sc. L.-A. Schäfer, Prof. Dr. N. H. Menzler, Prof. Dr.-Ing. O. Guillon  
Institute of Energy and Climate Research IEK-1: Materials Synthesis and Processing, Forschungszentrum Jülich GmbH (FZJ)  
Leo-Brandt-Str., 52425 Jülich (Germany)  
E-mail: m.ivanova@fz-juelich.de

Prof. Dr.-Ing. R. Peters, Dr.-Ing. M. Müller  
Institute of Energy and Climate Research IEK-14: Electrochemical Process Engineering, Forschungszentrum Jülich GmbH (FZJ)  
Leo-Brandt-Str., 52425 Jülich (Germany)

Dr. S. Haas, Dr. M. F. Seidler  
Institute of Energy and Climate Research IEK-5: Photovoltaics, Forschungszentrum Jülich GmbH (FZJ)  
Leo-Brandt-Str., 52425 Jülich (Germany)

Dr. G. Mutschke, Prof. Dr. K. Eckert  
Institute of Fluid Dynamics, Helmholtz-Zentrum Dresden Rossendorf (HZDR)  
Bautzner Landstraße 400, 01328 Dresden (Germany)

Dr. P. Röse, M.Sc. C. Gosselindemann, Dr.-Ing. A. Weber  
Institute for Applied Materials—Electrochemical Technologies (IAM-ET), Karlsruhe Institute of Technology (KIT)  
Adenauerring 20b, 76131 Karlsruhe (Germany)  
E-mail: philipp.roese@kit.edu

Dr. S. Calnan, Ing. R. Bagacki, Prof. Dr. R. Schlatmann  
Institute Competence Centre Photovoltaics Berlin (PVcomB), Helmholtz-Zentrum Berlin für Materialien und Energie GmbH (HZB)  
Schwarzschildstrasse 3, 12489 Berlin (Germany)

M.Sc. L.-A. Schäfer, Prof. Dr. N. H. Menzler, Prof. Dr.-Ing. O. Guillon  
Institute of Mineral Engineering (GHI), RWTH Aachen University  
Forckenbeckstraße 33, 52074 Aachen (Germany)

Prof. R. van de Krol, Dr. F. Liang, Dr. F. F. Abdi  
Institute for Solar Fuels, Helmholtz-Zentrum Berlin für Materialien und Energie GmbH (HZB)  
Hahn-Meitner-Platz 1, 14109 Berlin (Germany)  
E-mail: fatwa.abdi@helmholtz-berlin.de

Dr.-Ing. S. Brendelberger, Dr.-Ing. N. Neumann, Dr.-Ing. J. Grobbel, Dr. M. Roeb, Prof. Dr. C. Sattler  
Institute of Future Fuels, German Aerospace Center (DLR)  
Linder Höhe, 51147 Köln-Porz (Germany)  
E-mail: stefan.brendelberger@dlr.de

Dr.-Ing. I. Duran, M. E. C. Hofberger, Dr.-Ing. L. Stoppel, M. Sc. N. Uhlenbruck, Prof. Dr.-Ing. T. Wetzel  
Institute for Thermal Energy Technology and Safety (ITES), Karlsruhe Institute of Technology (KIT)  
Hermann-von-Helmholtz-Platz 1, 76344 Eggenstein-Leopoldshafen (Germany)  
E-mail: ines.duran@kit.edu

Dr.-Ing. B. Dietrich, Prof. Dr.-Ing. T. Wetzel  
Institute of Thermal Process Engineering (TVT), Karlsruhe Institute of Technology (KIT)  
Kaiserstraße 12, 76131 Karlsruhe (Germany)

Dr. D. Rauner, Prof. U. Fantz  
Augsburg University  
Universitätsstraße 1, 86159 Augsburg (Germany)

Dr. A. Hecimovic, Prof. U. Fantz  
Max-Planck-Institute for Plasma Physics  
Boltzmannstraße 2, 85748 Garching (Germany)  
E-mail: ursel.fantz@ipp.mpg.de

Dr. N. Kulyk, Prof. Dr. J. Harting  
Helmholtz Institute Erlangen-Nürnberg for Renewable Energy (IEK-11), Forschungszentrum Jülich GmbH (FZJ)  
Cauerstraße 1, 91058 Erlangen (Germany)  
E-mail: j.harting@fz-juelich.de

Prof. Dr. J. Harting  
Department of Chemical and Biological Engineering and Department of Physics, Friedrich-Alexander-Universität Erlangen-Nürnberg  
Cauerstraße 1, 91058 Erlangen (Germany)

© 2023 The Authors. Angewandte Chemie International Edition published by Wiley-VCH GmbH. This is an open access article under the terms of the Creative Commons Attribution Non-Commercial NoDerivs License, which permits use and distribution in any medium, provided the original work is properly cited, the use is non-commercial and no modifications or adaptations are made.



Mariya E. Ivanova studied Chemical Engineering and holds a PhD degree in the field of Materials Science (UCTM Sofia 2008). She leads the activities in the field of Proton Conducting Ceramic Fuel and Electrolysis Cells at the Institute of Energy and Climate Research IEK-1 of Forschungszentrum Jülich GmbH, Germany. Her research focus is on the development of proton conducting ceramic materials and electrochemical devices for demonstration and validation of various technologies, e.g., generation, extraction, purification and compression of H<sub>2</sub>. (Corresponding author for high-temperature electrolysis technologies and electrochemical compression.)



Ursel Fantz studied physics and received her PhD in electrical engineering in 1995. She is Head of the "ITER Technology and Diagnostics Division" at the Max-Planck-Institute for Plasma Physics, Garching and Professor at the University of Augsburg heading the Group "AG Experimental Plasma Physics". Her research focusses on low temperature plasmas physics and plasma technology for the conversion of abundant molecules into value-added chemicals, thus ranging from fundamentals to applications towards prototype developments combining physics with engineering issues. (Corresponding author for plasma conversion technology for H<sub>2</sub> generation.)



Fatwa F. Abdi is a group leader and the deputy head of the Institute for Solar Fuels, Helmholtz-Zentrum Berlin für Materialien und Energie GmbH. He obtained his PhD in Chemical Engineering from Delft University of Technology, the Netherlands, in 2013. He was the recipient of the Martinus van Marum prize from the Royal Dutch Society of Sciences and Humanities. His research focusses on the development of novel materials and engineering of devices for solar fuels production. (Corresponding author for photoelectrochemical water splitting.)



Stefan Brendelberger studied physics at the University of Karlsruhe and received his PhD in mechanical engineering at RWTH Aachen. He worked at the European Space Agency (Netherlands) and at the CSIRO Energy Centre (Australia). Currently, he is a team leader at the Institute of Future Fuels, German Aerospace Center DLR. His work focuses on technologies for the production of renewable fuels, thermochemical redox cycles for hydrogen production using concentrated solar radiation. In this area, he develops process concepts and performs experimental and numerical studies. (Corresponding author for thermochemical water splitting.)

components and performs experimental and numerical studies. (Corresponding author for thermochemical water splitting.)



Philipp Röse studied chemistry at Philipps University Marburg (Germany) and Lund University (Sweden). He obtained his PhD degree (2017) in the field of organic electrosynthesis. After working as a laboratory manager at TU Braunschweig, he started his independent research career at the Institute of Applied Materials—Electrochemical Technologies (IAM-ET) at the Karlsruhe Institute of Technology. His research focusses on the kinetic analysis of reaction and transport processes in electrochemical cells for water electrolysis, CO<sub>2</sub>

reduction and organic electrosyntheses. (Corresponding author for low-temperature electrolysis technologies, i.e. AWE, AEMWE, PEMWE.)



Ines Duran graduated in Chemical Engineering in 2014 from the University of Oviedo, Spain and received her PhD in 2019, with a work on adsorption processes for CO<sub>2</sub> capture at INCAR-CSIC. She is currently a postdoctoral researcher at the Karlsruhe Liquid Metal Laboratory (KALLA) at Karlsruhe Institute of Technology KIT. Her research focuses on hydrogen production via pyrolysis of methane based on liquid metal technology. (Corresponding author for pyrolysis based on liquid metal reactor technology.)



Jens Harting obtained his PhD in Physics at the University of Oldenburg in Germany in 2001. After extended periods in London (UK), Stuttgart (Germany), Eindhoven (The Netherlands) and Twente (The Netherlands), he joined the Helmholtz Institute Erlangen-Nürnberg for Renewable Energy and the Friedrich-Alexander-Universität Erlangen-Nürnberg in 2015. He leads the research department "Dynamics of Complex Fluids and Interfaces" and focuses on multi-scale modelling and simulation of complex fluids bridging from fundamental

material properties to applications in printable photovoltaics, fuel cells and electrolyzers. (Corresponding author for Simulation.)

for producing green H<sub>2</sub> with high-quality regarding purity, level of humidity and pressure is steadily increasing.

In order to cover certain quality requirements for further utilization, the produced H<sub>2</sub> usually requires further purification and compression. Although mature technologies for H<sub>2</sub> purification and compression are available at large scale, they have certain limitations. Adding any supplementary balance-of-plant (BOP) components for H<sub>2</sub> treatment to achieve the purity and pressure targets penalizes the overall structure of capital and operational expenditures (CapEx, OpEx) and the whole efficiency of the process chain. For these reasons, the establishment of novel technological pathways for producing sufficient amounts of highly pure, dry and compressed green H<sub>2</sub> has to be prioritized. Particularly interesting are the direct or indirect conversion of solar energy into H<sub>2</sub>, using power from photovoltaics, heat and power from concentrated solar facilities, or photons for photoelectrochemical water splitting.<sup>[2,3]</sup> These technological pathways are at the core of the Innovation Pool project “Solar H<sub>2</sub>: Highly Pure and Compressed” (i.e. H<sub>2</sub> produced from solar energy) and are the subject of the present review article. Biological and biocatalytic processes are beyond the scope of this review.

To achieve essential optimization of the complete process chain, it is necessary to evaluate (and possibly adapt within a tolerable range) the quality and suitability of the H<sub>2</sub> provided with regard to the relevant applications. Therefore, the present article will first give an overview of the quality requirements for H<sub>2</sub> with respect to its main fields of application. The paper will furthermore focus on the technologies using solar energy to produce H<sub>2</sub>, based on water splitting and bio-hydrocarbons cracking, and will highlight their technical advantages and limitations in terms of the achieved H<sub>2</sub> purity and pressure. Electrochemical H<sub>2</sub> separation and compression technologies will be briefly considered as well, along with the numerical simulations carried out on various scales as an overarching approach to support the technological development. Finally, a comparative summary of the technologies and an outlook will be provided.

## 2. Hydrogen Quality Requirements with Respect to Its Main Applications

H<sub>2</sub> is a valuable feedstock in various industrial fields such as steel production, chemical, cement and processing industries. In combination with carbon dioxide, hydrocarbons and synthetic fuels can be produced. H<sub>2</sub> is also utilized in households, various services and mobility. For all these purposes, conversion technologies such as chemical reactors, gas burners, internal combustion engines, gas turbines, fuel cells (Polymer Electrolyte Membranes—PEM, Solid Oxide—SOFC) are implemented (Figure 1). The standards for H<sub>2</sub> in terms of purity and level of compression differ considerably from one application to another one, and will be briefly outlined below.

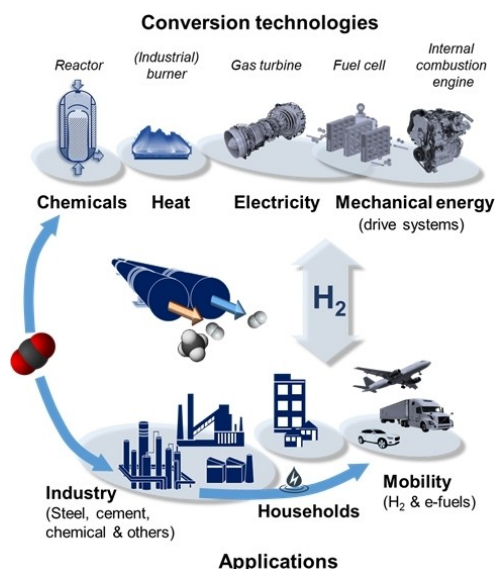


**Figure 1.** Principal sketch of hydrogen coupled to different conversion technologies and its usage in industry, households and mobility.

### 2.1. Hydrogen Purity for Various Applications

Multiple factors influence the purity of H<sub>2</sub>, e.g., production and conversion technology, but also distribution network (pipelines, tanks, etc.).

H<sub>2</sub> purity required for PEM fuel cells is defined within the standards SAE J2719, DIN EN 17124 and ISO 14687:2019. Figure 2 visualizes the maximum allowed concentration of impurities in ppm, according to the ISO standard. Generally, H<sub>2</sub> must offer purity of  $\geq 99.97\%$ , i.e. 300 ppm ( $\mu\text{molmol}^{-1}$ ) of non-hydrogen gases in total and  $1 \text{ mg kg}^{-1}$  particles. The major tolerated impurities are helium (He) up to 300 ppm or 100 ppm nitrogen and argon, and 200 ppm He. The next level of impurities encompasses water (5 ppm), oxygen (2 ppm), carbon dioxide (2 ppm) and

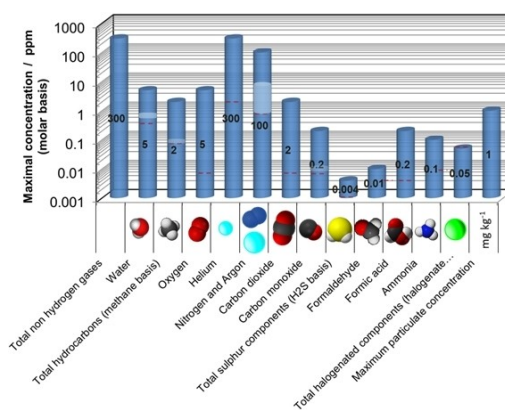


**Figure 2.** Hydrogen purity according to ISO standard (2012) 14687-2.2012 taken from Ohi<sup>[7]</sup> supplemented by fuel quality data from a Japanese hydrogen refuelling station (HRS) supplied by a natural gas (NG) steam reformer and data for the specific detection limit.

hydrocarbons (2 ppm), measured on methane basis. Some contaminants can only be tolerated at the sub-ppm level, defined as maximum concentrations: 200 ppb carbon monoxide, 200 ppb formic acid, 10 ppb formaldehyde, 4 ppb sulfur (monitored as H<sub>2</sub>S), 100 ppb ammonia and 50 ppb halogenates.

While the main contaminants in H<sub>2</sub> generated by PEM water electrolyzers (PEMWE) are water and oxygen, other contaminants such as nitrogen may be present as well.<sup>[4]</sup> Nitrogen is usually introduced as a result of purging, while a combination of O<sub>2</sub> and N<sub>2</sub> may result from leaks. Other trace contaminants such as ammonia and carbon dioxide may be introduced via the feed water, while halogens and sulphides may be due to corrosion of electrolyzer's components. The ISO 14687:2019 (Hydrogen fuel quality—product specification) and SAE J2719–202003 for Hydrogen Fuel Quality for Fuel Cell Vehicles (automotive)<sup>[5,6]</sup> stipulate hydrogen purity of ≥99.97% for fuel cells, of which a maximum of 5 ppm is allowed for either water or oxygen and 300 ppm for nitrogen.

## 2.2. Level of Hydrogen Compression for Various Applications

The compression of H<sub>2</sub> plays an important role in the value chain from its production to its use. Green H<sub>2</sub> produced from intermittent renewable solar energy (or other renewables) can balance seasonal fluctuations in renewable electricity production and must be stored for a continuous energy (or feedstock) supply to industry, households and transport applications. Figure 3 displays the pressure levels of H<sub>2</sub> in the supply chain for various industrial applications, grid injection, filling gas cylinders, refuelling station, etc. In the chemical industry, H<sub>2</sub> is used for ammonia production and for hydrogenation processes. Depending on the process conditions, the required pressure is between 60 to 300 bar. In the mobility sector, H<sub>2</sub> must be stored locally that can be realized in salt caverns at pressures between 60 and 200 bar. H<sub>2</sub> could be distributed via an expanded pipeline network at an operating pressure of 60 to 100 bar, similarly to the natural gas (NG) grid. H<sub>2</sub> storage for cars and trucks takes place at pressures of up to 700 bar for obvious space

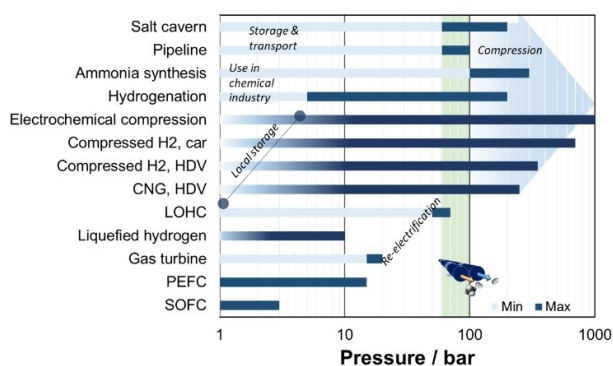


**Figure 3.** Pressure levels of hydrogen on the supply chain.

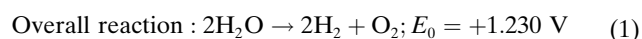
limitation reasons, while fuel cells operate at lower pressures, e.g., between 1 and 15 bar.

## 3. Assessment of Different Technologies for Hydrogen Production Driven by Solar Energy

As mentioned earlier, H<sub>2</sub> can be produced from solar power by direct utilization of sunlight to generate electrons or heat in processes such as photoelectrochemical water splitting (electrons), thermochemical water splitting (heat) and in liquid metal reactors (heat); or indirectly by i) PEMWE coupling to photovoltaic devices that convert the solar power to green electrons, or ii) supply from the grid (electricity, heat with large shares of solar power) to processes such as water electrolysis, liquid metal and plasma reactors. In the following chapters, direct and indirect technological pathways within the Innovation Pool project “Solar H<sub>2</sub>: Highly Pure and Compressed” are discussed in descending order of maturity.

### 3.1. Water Electrolysis

The most established family of technologies for producing green H<sub>2</sub> is water electrolysis, i.e. water splitting, powered by renewable electricity (Eq. 1).<sup>[8–12]</sup>



Electrolysis allows for energy storage, grid balancing and sector coupling via Power-to-X approach. Therefore, decreasing technology costs and providing flexibility to the power system are crucial aspects. This technology provides high-purity H<sub>2</sub> and is the most accessible to implement on a technical scale.

Based on the type of materials used in the device design and the process conditions, water electrolyzers can be systemized into alkaline (AWE: Alkaline Water Electrolysis; AEMWE: Anion Exchange Membrane Water Electrolysis) and acidic (PEMWE), functioning at temperatures below 100 °C (Figures 4, 5), or ceramic-based devices operating at higher temperatures (PCEC: 400–650 °C and SOEC: 700–900 °C, Figure 6).

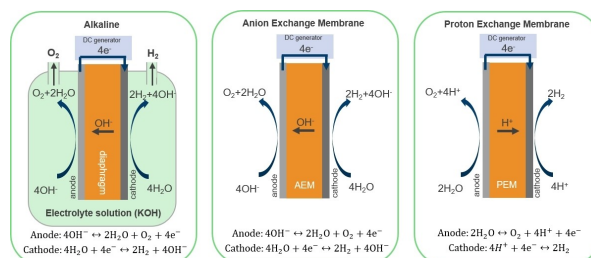


**Figure 4.** Low-temperature electrolysis technologies (redrawn after IRENA Report on Green H<sub>2</sub> cost reduction<sup>[13]</sup>).

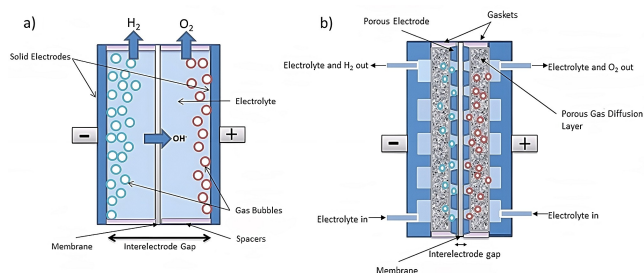


**Figure 5.** Schematic cell structure of the alkaline water electrolysis in a) classic and b) zero-gap design.<sup>[15]</sup> (Reprint permission by RSC Advances).

### 3.1.1. Alkaline Water Electrolysis (AWE)

This technology has a high degree of readiness (Technology Readiness Level (TRL) 8–9), and plants in the megawatt range have been existing for long time.<sup>[8–10]</sup> AWE is operated at temperatures in the range of 50 °C to 90 °C and pressures up to 30 bar.<sup>[14]</sup> As electrolyte, concentrated alkaline solutions are used. In classical AWE devices, the electrodes are separated by a diaphragm ( $\approx 0.5$  mm) that is permeable to water and hydroxide ions (Figure 5a).<sup>[15]</sup> Thus, the crossover of hydrogen and oxygen is reduced, resulting in high H<sub>2</sub> purity ( $\approx 99.8\%$ ) and device efficiency.<sup>[16–21]</sup> Compared to the PEMWE technology, the requirements for electrolyte purity are lower and catalysts, as well as diaphragms are more robust.<sup>[22]</sup> However, the classical AWE suffers from low current densities and efficiencies in a stack ( $< 0.4$  A cm<sup>-2</sup>;  $\approx 60$ – $70\%$ ).<sup>[14,23–26]</sup> The clear advantage of AWE is the reduced cost due to the use of abundant non-noble metal catalysts based on Ni, Co, Fe and Mo.<sup>[27–39]</sup> The lifetime of AWE devices is longer and the related maintenance costs are considerably lower compared to other well-established technologies.<sup>[8,10,14,40–42]</sup>

Modern designs of AWE follow a zero gap approach,<sup>[43,44]</sup> thereby such offer higher current densities and efficiencies at beneficial cost.<sup>[45]</sup> In this case, the diaphragm is replaced by a thinner ( $< 0.2$  mm) polymer membrane (Figure 5b<sup>[15]</sup>). Since almost no gas is generated between the two electrodes, gas crossover is advantageously reduced compared to the conventional design.

In the so-called Anion Exchange Membrane Water Electrolysis (AEMWE, TRL 2–4), a hydroxide ion conducting membrane (e.g., Fumasep<sup>®</sup> FAS-50 or FAPQ, AMI 7001, etc.) is sandwiched between the porous electrodes.<sup>[46–51]</sup> Current research in AEMWE focuses on increasing the operation lifetime of the membrane and improving the gas transport in the microporous layers.<sup>[52,53]</sup>

The purity of H<sub>2</sub> produced is typically more than 99.9%, while for O<sub>2</sub> is in the range of 99.0 to 99.5%<sup>[54]</sup> and both can be increased to 99.999% by catalytic gas purification systems.<sup>[54]</sup> Since the two product gases can form explosive mixtures, an emergency shutdown of the entire electrolyzer system at a mixing threshold value of 2 vol.% is common for safety reasons.<sup>[55,56]</sup> In addition, the gas crossover leads to a reduction in the overall efficiency due to undesired side

reactions. To ensure continuous electrolysis operation, it is therefore essential to keep the contamination of the product gas as low as possible during operation. However, operation in the very low partial load range ( $< 20\%$  of total power) must be avoided as it is more critical in terms of gas contamination and safety risks. This makes implementation into the existing renewable energy-based power grid a very challenging task. Higher current densities simultaneously lead to an increase in heat production, mainly due to activation overvoltages, which in turn increases gas impurities. In order to achieve the highest possible gas purity and energy efficiency in electrolysis, all cell components, materials and process parameters must be precisely matched to each other.<sup>[11,57,58]</sup>

Another important process parameter is the pressure, as the subsequent compression of the gases is energy-intensive and significantly reduces the overall efficiency of the process. Commercial systems nowadays, such as those from Enapter, typically operate at pressures between 8 and 35 bar.<sup>[59]</sup> Increasing the pressure has no effect on the H<sub>2</sub> production rate,<sup>[10,60–62]</sup> but more gas dissolves in the electrolyte,<sup>[58]</sup> resulting in higher concentration gradients for diffusion through the separator and finally to more impurities. The gas contamination can be reduced considerably if the mixing of anolyte and catholyte is carefully avoided during operation.

### 3.1.2. Polymer Exchange Membrane Water Electrolysis (PEMWE) and Coupling with Photovoltaic Facilities (PV)

PEM electrolysis (TRL 8–9) is operated with pure water and current densities in the range of 2 A cm<sup>-2</sup>/1.7 V with efficiencies larger than 72%<sup>[43]</sup> (up to 4 A cm<sup>-2</sup> still possible at high efficiencies). The polymer exchange membrane is gas-tight, unlike the diaphragms in alkaline electrolysis. However, to achieve the desired protonic conductivity, water must be absorbed on molecular level by sulfonic acid functional groups in the Nafion<sup>®</sup> membrane backbone. Precious metals such as iridium (Ir) are usually utilized as catalysts to improve H<sub>2</sub> purity at the cathode, as the permeating oxygen is converted directly into water.

The operation of the electrodes at different pressure levels, especially at the cathode, is thermodynamically beneficial and no additional compression is necessary. The average pressure in commercial electrolyzers is between 30 and 40 bar, while pressures of above 500 bar are technically possible, however still at an early stage of development and hardly considered industrially.<sup>[63]</sup> The gas composition at the cathode is not affected by the pressure, as the permeating oxygen is reduced electrochemically or it reacts catalytically with hydrogen at the platinum (Pt) catalyst to form water.<sup>[25]</sup> In the case of thin membranes ( $< 180$   $\mu$ m), a recombination catalyst is required at the anode to ensure hydrogen in oxygen concentrations of less than 2%<sup>[64]</sup> or an immediate dissolution in air.<sup>[65]</sup>

The operating conditions of PEMWE make this technology ideal for coupling with photovoltaic (PV) facilities.<sup>[66]</sup> The electricity harvested from the PV systems can be

transferred to the PEM electrolyzers by direct coupling and by DC-DC conversion (DC: direct current). Both approaches aim to keep the operating point of the PV modules close to their maximum power point (MPP). In order to match the properties of the PV system and the electrolyzer in a directly coupled system, the number of PV and electrolysis cells connected in series can be varied. Direct coupling allows for highest efficiencies under laboratory conditions. Together with highly efficient multi-junction concentrator solar cells, this approach has enabled efficiencies of up to 30 % in the conversion of solar energy to H<sub>2</sub> (Solar-To-Hydrogen STH,  $\eta_{\text{STH}}$ ),<sup>[67,68]</sup> and about 18 % in small-scale outdoor tests (single PV cell).<sup>[69]</sup> Excellent results have been also demonstrated in large-scale tests (PV power  $P_{\text{PV}}=100$  s of W up to 20 kW) with commercially available Si-based solar cells.<sup>[70–75]</sup> For such a coupling, energy efficiency of 94 % relative to the potential energy output at MPP has been reported in long-term operation<sup>[76]</sup> under varying solar irradiance and ambient temperature conditions. The varying conditions mainly lead to a change in the I–V characteristic of the PV part, so that optimizations need to be considered.<sup>[77]</sup> The second main coupling strategy utilizes DC-DC conversion and MPP tracking electronics to further optimize H<sub>2</sub> production.<sup>[78–82]</sup> Since modern DC-DC converters are highly efficient (96–99 %<sup>[83]</sup>), their use can be a worthwhile trade-off in terms of overall system efficiency, especially under conditions, for which direct coupling is not optimal (e.g., partial shading of the PV installation). DC-DC converters add upfront cost,<sup>[72,80]</sup> while potentially reducing wiring cost and increasing flexibility.<sup>[83,84]</sup> In-depth analysis of these two approaches to leveled H<sub>2</sub> costs are rare, however, 3–6 % advantage in H<sub>2</sub> production cost was indicated for the direct coupling technology.<sup>[76]</sup>

### 3.1.3. Solid Oxide Cell Based Water Electrolysis

A key technology offering the highest efficiencies for H<sub>2</sub> production is the Solid Oxide Cell (SOC) based water electrolysis. SOC refers generally to two types of ceramic electrochemical cells: i) Solid Oxide Electrolysis Cell with an oxygen ion conducting electrolyte (SOEC, Figure 6, right) and ii) Proton Conducting Electrolysis Cell with a proton conducting electrolyte (PCEC, Figure 6, left).

The main difference between an SOEC and a PCEC entails in the type of charge carriers diffusing across the solid electrolyte, being oxygen ions and protons, respectively. This results in a different operation principle and temperature, as well as specific materials that constitute the cells, and, above all, the final purity of the H<sub>2</sub> produced. In the case of an SOEC, the H<sub>2</sub> purity achieved without further purification is  $\leq 99.9\%$  (value based on estimation<sup>[40]</sup>), while in the case of a PCEC, H<sub>2</sub> with purity  $\geq 99.97\%$  can be produced directly.<sup>[85]</sup>

The major advantage of SOCs based electrolysis over low-temperature technologies is the high theoretical energy efficiency. An ideal system could achieve 100 % efficiency if the heat produced by internal losses is fully kept in the system (no heat dissipation and other losses) and used for

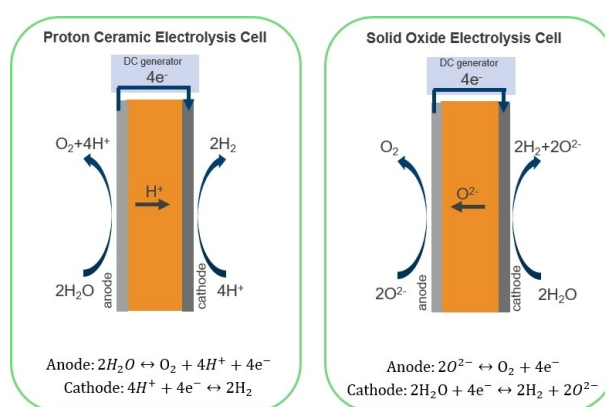


**Figure 6.** Solid Oxide Cells for high-temperature water electrolysis: PCEC based on a proton conducting solid electrolyte (left) and SOEC based on an oxygen ion conducting solid electrolyte (right). (SOEC: redrawn after IRENA Report on Green H<sub>2</sub> cost reduction<sup>[13]</sup>).

the endothermal water electrolysis reaction (the so-called thermoneutral operation). However, in a real system, heat losses and non-ideal heat exchangers cannot be avoided, so more heat is required. Depending on the cell design, SOEC operation at 1.5 V might result in a rather high current density and subsequent cell degradation. In this case, other heat sources such as electrical heaters, solar heaters or industrial heat are required. If all the necessary heat is supplied from an external source providing waste heat to substitute electrical energy for steam production, heating of educts and reaction heat, an efficiency (that is only considering the electrical input) of above 100 % is possible without seriously affecting the cell under harsh load conditions. An efficiency of  $\approx 100\%$  is already achieved when taking into account the Higher Heating Values (HHV) of hydrogen (84 % Lower Heating Values (LHV)) for actual SOEC-systems fed with steam/heat from other industrial processes (e.g., steel industry, such as the Sunfire System at Salzgitter Flachstahl GmbH, Germany).

SOCs can furthermore operate reversely switching between fuel<sup>[86]</sup> and electrolysis cell mode,<sup>[87]</sup> which is useful for H<sub>2</sub>-based energy storage systems. SOC are not limited to H<sub>2</sub> fuel: they can be fed with reformat gas mixtures, ammonia or even internally reform hydrocarbons.<sup>[88–90]</sup> In the electrolysis mode, syngas or carbon monoxide can be produced for subsequent chemical processes applying electricity and heat from solar power.<sup>[91–93]</sup>

The combination of SOEC and concentrated solar technology was intensively investigated already in the past decades<sup>[94–97]</sup> and more recently.<sup>[98–102]</sup> These recent works provide a solid experimental evidence for the concept, showing that operating SOEC with solar heat is feasible and promising. Since PCEC technology is not yet so mature, very few data could be found on the integration of proton conducting cell with solar power. However, the work by Ghosh et al.<sup>[103]</sup> provides insights into the integration of a proton conducting fuel cell (PCFC) rather than a PCEC.

### 3.1.3.1. Solid Oxide Electrolysis Cells (SOEC)

SOECs (TRL 6–7) usually operate in the range of 700–900 °C,<sup>[104]</sup> at which sufficient level of ionic conductivity in the solid oxide electrolyte is achieved (considering technically feasible electrolyte thicknesses). The high operating temperatures enable the use of cost-saving, precious metals-free electrocatalysts. On the other hand, thermally activated aging is accelerated, so current research is aimed at lowering the temperature.<sup>[105]</sup> This additionally expands the possibilities of a more cost-effective material selection for stack and peripheral components, e.g., for interconnects, heat exchangers, etc.

Material selection for SOEC cells and stacks is based on chemical and thermomechanical compatibility with the solid electrolyte, i.e. fluorites, perovskites, etc.<sup>[106]</sup> Zirconia-based electrolytes fulfil the requirements for negligible electronic conductivity, which is not the case for alternative electrolytes such as Gd- or Sm-doped ceria.<sup>[104]</sup> Fuel electrodes conventionally consist of a cermet of nickel and one of the aforementioned electrolyte materials. The main challenges are associated with achieving high electrocatalytic activity, ionic conductivity and low degradation at the same time. Common air electrodes are perovskite-type lanthanum manganites, ferrites and cobaltites.<sup>[104,107–109]</sup>

Due to the all-solid-nature of SOECs, various designs could be developed in last decades. Planar types consisting of flat multi-layer structures are the most common type nowadays,<sup>[104]</sup> in addition to (micro–) tubular designs, being electrolyte-supported (ESC), fuel electrode-supported (ASC) and metal-supported cells (MSC).<sup>[86,110–112]</sup>

To obtain technically meaningful current and voltage levels for a system, individual cells are connected in series in a stack. In planar SOEC stack design, the cells are stacked between metallic interconnectors, that ensure bipolar contact with the electrodes of the neighboring cells. Contacting and gas supply are realized by flowfield structures, while protective coatings are required to prevent corrosion of the metallic interconnects and reduce Cr evaporation, that is harmful for the steam electrode. Glass, glass-ceramics, metallic solders or compressive gaskets are applied for a gas-tight seal. In the case of tubular stacks, different designs are available. Mostly, the cells are monopolar contacted, which leads to additional in-plane losses along the electrodes.

Operando characterization,<sup>[87,113,114]</sup> data analysis and modelling approaches<sup>[86,115–117]</sup> on different scales are mandatory to understand the electrochemical processes in the cells and stacks and to improve their performance and durability.<sup>[117–120]</sup>

Various SOEC cell and stack designs have been used in commercial or pre-commercial SOFC-systems. The largest market to date is the Combined Heat and Power (CHP) systems developed by various companies.<sup>[121–130]</sup> Even though most of these companies have started developing cells, stacks and systems for SOEC-applications, the number of commercially available high-temperature electrolyzers remains limited. An example is the Sunfire SOEC-systems<sup>[126,131]</sup> with H<sub>2</sub> production rate of 750 Nm<sup>3</sup> h<sup>-1</sup> at up

to 850 °C, conversion efficiencies above 84 %, a consumption of 3.6 kWh<sub>N</sub><sup>-3</sup> produced H<sub>2</sub> with purity above 99.95 % after an additional purification stage, Figure 7.

While SOFC lifetimes of 4–10 years have been achieved with different cells, stacks and systems, the proven lifetimes of SOECs are mostly below 20 kh,<sup>[132]</sup> which is mainly related to the fact that the intensive SOEC development only started in the last decade. The straightforward approach of using SOFC cells and stacks for SOEC applications has proven to be critical in terms of lifetime and durability. Thus, new electrode, cell and stack concepts for electrolysis operation are being developed. In addition, another research focus is on improvements at the system level, e.g., through external heat coupling<sup>[133]</sup> or reduced water quality requirements (seawater).<sup>[134]</sup>

The operation of pressurized SOCs offers advantages in terms of power density, but even more in terms of the use of pressurized off-gas. A number of pressurized systems combining an SOFC-stack with a gas turbine have demonstrated an increased system efficiency [Siemens,<sup>[135]</sup> MHI<sup>[121]</sup>] but also higher complexity, which makes system control more difficult and can even lead to severe failures. Larger SOEC-systems for the production of H<sub>2</sub> have so far been operated at atmospheric pressure.<sup>[136]</sup> Compared to the numerous results for atmospheric operation, the experimental results under elevated pressure are limited so far. Increasing the pressure at temperatures of up to 900 °C leads to problems with sealing and pressure regulation<sup>[137]</sup> as the ceramic cells can hardly withstand pressure gradients between air and fuel gas. In small-scale cells and stack tests, the operating pressure has been usually set in a range of ≈ 1 to 10 bar.<sup>[138–143]</sup>

### 3.1.3.2. Proton Conducting Electrolysis Cells (PCEC)

Although the early indications on their potential could be traced back to the 1980s,<sup>[144–146]</sup> the maturity of proton conducting cell (PCC) technology (TRL 2–4) trails behind that of SOECs. Due to its inherent advantages, this technology marks nowadays accelerated development.<sup>[147]</sup> Several key differences from conventional low- and high-temperature technologies make PCEC a potentially viable technology for rapid market penetration at reduced CapEx/OpEx costs.

Since PCECs consist of proton conducting ceramic materials, they operate effectively in the temperature range



Figure 7. Sunfire SOEC-HyLink system<sup>[131]</sup> (graphics with permission from Sunfire).

of 400–650 °C,<sup>[148,149]</sup> which alleviates degradation issues and leads to a flexible stack design with simpler maintenance, disassembly and recycling. Additionally, cheaper interconnects can be used and no precious metal catalysts are required (compared to SOEC and PEMWE). Furthermore, PCECs produce dry and clean H<sub>2</sub> (see product side of PCEC in Figure 6 (left)) ready for compression, transport, utilization or storage. Cells based on proton conducting ceramics can be integrated into a solar thermal power generation system.<sup>[103]</sup> In addition to that, the balance-of-plant can be kept simpler, which in turn affects the cost efficiency (e.g., H<sub>2</sub> purification technologies account for up to 14 % and 30 % of the total discounted capital and operating costs, respectively<sup>[150]</sup>) and the final price of the product.<sup>[151]</sup>

The PCEC's feature for instantaneous generation of clean, dry H<sub>2</sub> that can be readily compressed by pressurized operation or downstream compression can have major implications for coupling with other processes and sectors. To achieve a technically suitable level of H<sub>2</sub> compression for a range of applications, PCEC technology can be coupled with PEM electrochemical compressors (PEM-EHC). PEM-EHC technology requires excellent H<sub>2</sub> purity and certain pre-compression, both of which can be achieved with PCECs (up to 5–12 bars<sup>[152]</sup> currently, H<sub>2</sub> purity of  $\geq 99.97\%$ <sup>[85]</sup>).

PCCs are typically based on B-site substituted BaZrO<sub>3</sub>–BaCeO<sub>3</sub> (BZC) solid solutions as electrolyte, BZC: Ni-based cermet<sup>[148,153]</sup> as H<sub>2</sub> electrode, and Co-, Fe-, Mn-, Pr-rich perovskites serving as air/steam electrodes.<sup>[154–156]</sup> Research and development activities are usually aimed at overcoming problems related to cell performance, durability<sup>[154,157]</sup> and scalability. Reports on PCC steam electrolysis are sparse and often limited to button cells ( $\approx 1$ –1.5 cm<sup>2</sup>).<sup>[157,158]</sup> Recently, the design of planar cells has been improved and scaled up,<sup>[159–166]</sup> with faradaic efficiencies of, e.g., 82–85 % or more at 600 °C and sizes up to 25 cm<sup>2</sup>, while for some other applications (e.g., hydrocarbon dehydrogenation), symmetric cells of up to 140 cm<sup>2</sup> were reported.<sup>[161,167]</sup> Tubular PCECs with improved anode design<sup>[154]</sup> have demonstrated stable operation and promising faradaic efficiency at high steam pressures. H<sub>2</sub> production rates

approach the predicted range of PCEC operation and exceed those of SOEC operation below 650–700 °C.

Although significant progress has been achieved at the materials and cell fabrication level, there is still an essential gap at the stack and system levels. Recently, the integration of PCCs into a 0.5 kW-scale stack<sup>[168]</sup> and the operation of PCC under pressure conditions (H<sub>2</sub> compression up to 12 bar)<sup>[152]</sup> have been demonstrated. However, systematic data on cell performance, including pressure conditions, design of durable sealants and interconnects, stacking concepts, BOP, life cycle assessment (LCA) and techno-economic analysis (TEA) of PCEC technology in conjunction with end-user cases are still very scarce. Finally, there is also very little data on degradation effects, while modelling efforts to support stack and system design are insufficient, as are the safety and recycling aspects associated with this technology.

### 3.1.4. Summarizing Remarks on Water Electrolysis

A direct comparison of the water electrolysis technologies is provided in Table 1, which summarizes the state-of-the-art (SoA) Key Performance Indicators (KPIs) of the low- and high-temperature water electrolysis technologies. Data on AWE, AEMWE, PEMWE and SOEC are collected according to,<sup>[169]</sup> while data on PCEC are not available. As it can be inferred from the table, the TRL is reflected in the collected performance, durability and cost data.

### 3.2. Photoelectrochemical Water Splitting (PEC)

Photons from sunlight can be used to split water directly into H<sub>2</sub> and O<sub>2</sub> in a process called photoelectrochemical (PEC) water splitting. This process uses semiconductor photoelectrodes immersed in aqueous electrolytes (Figure 8). The typical operation temperature range of PEC devices is 20–80 °C.<sup>[170]</sup>

**Table 1:** Comparison of “State-of-the-Art Key Performance Indicators, 2020” (SoA-KPIs) summarized for low- and high-temperature water electrolysis technologies based on data in the Seed Paper on H<sub>2</sub> production by the European Research Area (ERA).<sup>[169]</sup> Data about PCEC are not available.

SoA KPIs 2020	AWE	AEMWE	PEMWE	SOEC
Nominal current density [A cm <sup>-2</sup> ]	0.2–0.8	0.2–2.0	1.0–2.0	0.3–1.0
Voltage range (limits) [V]	1.4–3.0	1.4–2.0	1.4–2.5	1.0–1.5
Operating temperature [°C]	70–90	40–60	50–80	700–850
Cell pressure [bar]	< 30	< 35	< 30	1
Voltage efficiency (LHV) [%]	50–68	52–67	50–68	75–85
Electrical efficiency (stack) [kWh kg <sup>-1</sup> [H <sub>2</sub> ]]	47–66	51.5–66	47–66	35–50
Electrical efficiency (system) [kWh kg <sup>-1</sup> [H <sub>2</sub> ]]	50–78	57–69	50–83	40–50
Lifetime (stack) [kh]	60	> 5	50–80	< 20
Stack unit size [kW]	1000	2.5	1000	5
Electrode area [cm <sup>2</sup> ]	10 000–30 000	< 300	1500	200
Cold start (to nominal load) [min]	< 50	< 20	< 20	> 600
Capital costs (stack) minimum 1 MW [USD kW <sup>-1</sup> ]	270	Unknown	400	> 2000
Capital costs (system) minimum 1 MW [USD kW <sup>-1</sup> ]	500–1000	Unknown	700–1400	Unknown

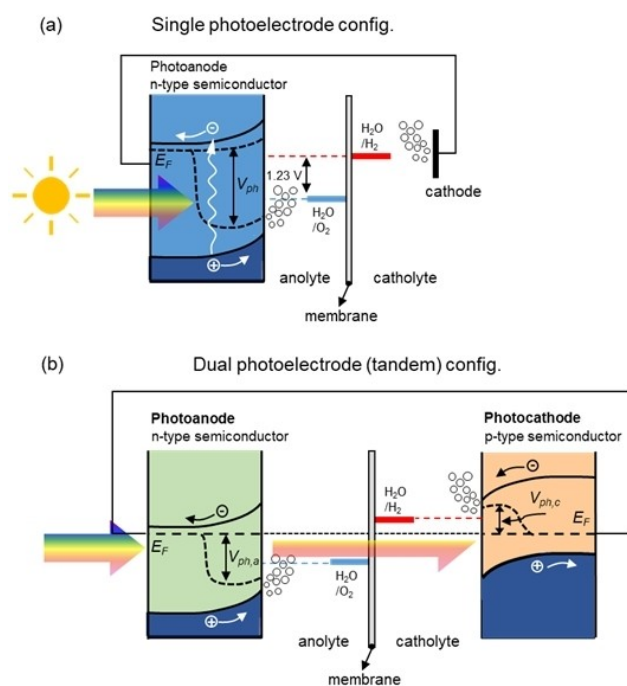


**Figure 8.** Schematic representation of photoelectrochemical water splitting in a device with (a) a light-absorbing semiconductor photoanode and a dark cathode, and (b) two light-absorbing semiconductors serving as photoanode and photocathode.  $E_F$  = Fermi level,  $V_{ph}$  = photovoltage,  $V_{ph,a}$  = anode photovoltage,  $V_{ph,c}$  = cathode photovoltage.

Compared to indirectly coupled photovoltaic (PV) cells with electrolyzers, PEC water splitting offers several advantages. First, the integration of the light absorber with the electrocatalyst significantly improves thermal management. For a hypothetical solar fuel generator with an energy conversion efficiency of 20% and optical reflection losses of 10%, 70% of the incident solar radiation is converted into heat. For photovoltaic devices, this can lead to operating temperatures of 60–80 °C and thermally induced efficiency losses of 10% or more within the semiconductor.<sup>[171]</sup>

In PEC devices, such detrimental temperatures are not reached because the surrounding water acts as a natural coolant. Moreover, any temperature increase will both reduce the thermodynamically required voltage for water splitting (by 8.5 mV per 10 °C for liquid water) and will enhance the electrochemical reaction kinetics. Secondly, PEC devices have much lower operating current densities (10–20 mA cm<sup>-2</sup>) than commercial water electrolyzers (0.5–2 A cm<sup>-2</sup>). This greatly lowers the requirements for the electrocatalysts and may enable the use of earth-abundant materials.<sup>[172–175]</sup> To illustrate this, current densities of 10 mA cm<sup>-2</sup> have been achieved at overpotentials of ≈50 and ≈400 mV for hydrogen and oxygen evolution, respectively, using earth-abundant materials like NiMo, NiSe<sub>2</sub>, NiFeO<sub>x</sub>, and CoO<sub>x</sub>.<sup>[176–178]</sup> This corresponds to an electrochemical water splitting efficiency of ≈75%, considering the LHV of hydrogen, which is comparable to that of iridium/

platinum-catalyzed PEM electrolyzers at much higher current densities of ≈1 A cm<sup>-2</sup> (see section 3.1.2).

Several classes of materials have been investigated as light-absorbing semiconductors in PEC water splitting devices. Devices based on high-quality PV-grade III–V semiconductors have demonstrated the highest efficiencies<sup>[179–181]</sup> (19% STH efficiency reported<sup>[179]</sup>). Devices based on relatively low-cost and stable oxide semiconductors, often combined with Si, have also been reported, but show lower efficiencies (8%).<sup>[182–184]</sup>

Efforts are increasingly focused on scaling up PEC devices to sizes beyond the laboratory-scale (<1 cm<sup>2</sup>). For example, a BiVO<sub>4</sub>/Si-based device with a photoactive area of 50 cm<sup>2</sup> and a WO<sub>3</sub>/DSSC-based device (≈130 cm<sup>2</sup>) have been reported, both with efficiencies of ≈2%.<sup>[185,186]</sup> Similar efficiencies have been achieved with a large modular BiVO<sub>4</sub>-based device with a photoactive area of 6,400 cm<sup>2</sup>.<sup>[187]</sup> In all these demonstrators, the efficiency was limited by losses related to mass transport, which are difficult to avoid when increasing the area. Another approach to scale-up the size is to increase the irradiation intensity by concentrating the sunlight. However, the much higher power at which the PEC device operates, the more stringent demands on its design. The highest demonstrated output power of a PEC water splitting device is ≈27 W under 474-sun concentration with efficiency of ≈15% and H<sub>2</sub> production rate of ≈1 g h<sup>-1</sup>.<sup>[188]</sup>

As mentioned above, most practical applications and processes using H<sub>2</sub> require H<sub>2</sub> at elevated pressure. To the best of our knowledge, there are currently no reports (experimental or numerical) of PEC devices at elevated pressure. This is likely due to the relatively low readiness (TRL 5) of PEC water splitting systems.<sup>[188–191]</sup>

The purity of the H<sub>2</sub> produced from PEC water splitting demonstrators is not usually reported. Faradaic efficiency for H<sub>2</sub> production is the most commonly reported performance parameter (usually close to 100%), but the amount of impurities in the H<sub>2</sub> product stream is often not analyzed. However, some indications can be found that a fully monolithically integrated PEC water splitting device based on tandem III–V absorbers, earth abundant co-catalysts and anion exchange membranes can produce hydrogen of ≥98% purity (≤2% oxygen crossover).<sup>[192]</sup> Hydrogen purity above 94% and H<sub>2</sub> production rate of 200 g h<sup>-1</sup> have been reported for a 100 m<sup>2</sup> photocatalytic solar hydrogen production plant.<sup>[193]</sup>

There are two general design considerations relevant to elevated pressure and high purity operation as furthermore discussed: i) membrane vs. membraneless, and ii) liquid vs. vapor electrolyte.<sup>[194]</sup> Similar to electrolyzers, ion exchange membranes are often used in PEC water splitting devices to avoid mixing of products and to achieve high H<sub>2</sub> purity. Bipolar membranes (BPM) have also been utilized in several devices,<sup>[195–197]</sup> allowing for the use of anolytes and catholytes with different pH.<sup>[198–200]</sup> Membraneless devices have also been proposed and demonstrated, using either an optically transparent porous separator<sup>[201,202]</sup> or electrolyte velocity control.<sup>[203–206]</sup>

In terms of the type of electrolytes used in PEC water splitting devices, liquid electrolytes are far more common, but there are several reports on units fed with water vapor. It has been argued that vapor-fed PEC devices offer several potential advantages. Firstly, the absence of a liquid phase helps to suppress photo-corrosion, as corrosion products remain near the surface and would therefore be more likely to redeposit. Secondly, no bubbles are generated, so all bubble-related losses (e.g., scattering of light, blocking of active sites) can be avoided. Finally, in certain geographical locations with sufficient relative humidity, the device can simply be fed with (humid) ambient air. It has been shown that PEM electrolyzers can operate with higher efficiency when fed with water vapor, especially in the range of relatively low current densities, i.e. tens of  $\text{mA}\cdot\text{cm}^{-2}$ , which is relevant for (non-solar concentrating) PEC devices.<sup>[207]</sup> Iwu et al. were among the first to report such a configuration with a  $\text{TiO}_2$ -based photoelectrode, albeit achieving relatively low photocurrents.<sup>[208,209]</sup> Xu et al. also investigated the performance of a PEC cell under asymmetric conditions, where the anode compartment was supplied with air of 80% relative humidity (RH) and the cathode with dry argon. Unfortunately, no  $\text{H}_2$  could be detected, mainly due to the low current densities and the fact that the proposed system was a continuous flow reactor rather than a batch type reactor.<sup>[210,211]</sup> A STH efficiency of 7.5% was demonstrated with a III–V photocathode-based device.<sup>[212,213]</sup> These reports suggest that a vapor-fed compact, monolithic cell concept offers an interesting possibility for PEC water-splitting devices operating under elevated pressure.

Since PEC devices depend foremost on the efficient utilization of solar photons, optical losses by bubble formation must be taken into account.<sup>[214,215]</sup> Gas bubbles diffract and scatter light and therefore affect the number of photons reaching the absorber(s) when illuminating through the electrolyte. Increasing the pressure would reduce the bubble density (i.e. the number of bubbles per unit area) due to a higher nucleation rate.<sup>[214,215]</sup> To make a first-order estimate of the optical losses, we use the empirical pressure-dependent relationships of bubble diameter and density of  $\text{H}_2$  and  $\text{O}_2$  reported by Sillen at  $200\text{ mA}\cdot\text{cm}^{-2}$  current density,<sup>[215]</sup> which are plotted in Figure 9a and b. The optical losses plot as a function of pressure in Figure 9c clearly illustrates the advantages of operating at higher pressure. This impact is greater for  $\text{O}_2$  bubbles due to the larger pressure dependence of the bubble diameter (Figure 9a); by increasing the pressure from 1 to 10 bars, the optical losses can be reduced from 17% to about 7–8%. In addition, the decrease in total bubble volume (or void fraction in the electrolyte) with increasing pressure boosts the electrolyte conductivity and reduces the ohmic losses.<sup>[216–218]</sup>

Product separation and purity are also affected by the increase in pressure. In membraneless devices, these aspects are affected by characteristics and dynamics of the bubbles, especially considering that the PEC device is tilted towards the sun. While the addition of a membrane would prevent direct crossover, some crossover may still occur due to diffusion of dissolved  $\text{H}_2$  and  $\text{O}_2$  through the membrane<sup>[221,222]</sup> (more pronounced at higher pressures). By

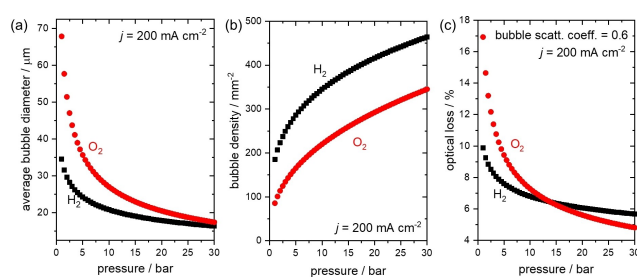


**Figure 9.** (a) Average bubble diameter and (b) bubble density of  $\text{H}_2$  and  $\text{O}_2$  as a function of pressure at  $200\text{ mA}\cdot\text{cm}^{-2}$ , obtained from the empirical relationship reported by Sillen;<sup>[215]</sup> (c) Optical losses due to (single-event) light scattering at  $\text{H}_2$  and  $\text{O}_2$  bubbles as a function of pressure, calculated based on the equation in<sup>[219,220]</sup> and the dataset in (a) and (b). Note that a 10% optical loss means that the overall solar-to-chemical energy conversion efficiency of the PEC device would be reduced by 10%. The bubble scattering coefficient is assumed to be 0.6 and independent of pressure. This representation is for illustrative purposes only, as the complete relationship between optical loss and pressure is likely to be more complex.

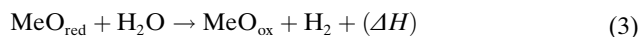
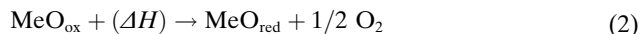
using a membrane, the anolyte and catholyte can be operated at different pressures, which can be beneficial since only  $\text{H}_2$  and not  $\text{O}_2$  needs to be pressurized. Operation at higher pressure requires the selection of appropriate materials/components for the device construction. In addition to the mechanical requirements, some components must also have high optical transparency (e.g., optical window).

These considerations show that while high pressure PEC cells are a potentially attractive proposition, the concept has not yet been explored in detail. The performance of photoelectrodes and/or catalysts at elevated pressure has yet to be determined, including their activity, stability and durability. In addition, the optimal device architecture for operation at elevated pressures may be very different from the common architectures used for atmospheric pressure. Ideally, the internal volumes need to be as small as possible. At the same time, sunlight needs to be collected over large areas to increase the production rate of  $\text{H}_2$ <sup>[223]</sup> or using parabolic mirror in order to collect sunlight over a larger area into a more compact PEC device.<sup>[188,224]</sup> A decoupled system design, where  $\text{O}_2$  and  $\text{H}_2$  generation is done separately, is also an option.<sup>[225,226]</sup> However, these configurations typically operate at higher current densities, at which the product crossover may become an issue.<sup>[227,228]</sup> Auxiliary components (e.g., pressure regulator, pumps) that can operate at elevated pressure also need to be included in the design, typically adding to the complexity and cost of the overall system. An optimal range of operation pressure should be quantitatively identified and used as a key design parameter for elevated-pressure PEC water splitting devices.

### 3.3. Thermochemical Water Splitting (TCWS)

$\text{H}_2$  production by thermochemical water splitting (TCWS) has been discussed in literature for several decades (TRL 5).<sup>[229]</sup> Thermochemical water splitting cycles use two or more reactions to split water into  $\text{H}_2$  and  $\text{O}_2$ . In comparison

to the direct water thermolysis ( $T \geq 2200^\circ\text{C}$ ),<sup>[229]</sup> the maximum process temperature is significantly reduced by utilizing two-step redox cycles. In the first step, a metal oxide is thermally reduced at high temperatures, while in the second step the reduced oxide contacts with water and hydrogen is released (Eq. 2, 3). Cycles with three and more steps have also been proposed.<sup>[230]</sup>



For solar driven thermochemical cycles, concentrated solar energy provides the heat necessary for the reduction reaction (Figure 10). The so-called receiver-reactors are often applied as the core component of such a system. Therefore, most efforts in this field have been focused on the exploration of suitable redox materials and the related processes, but also on the development of suitable receiver-reactors.

In recent years,  $\text{CeO}_2$  has become the reference redox material for solar thermochemical water splitting cycles<sup>[232,233]</sup> due to its cycling stability, high selectivity and fast kinetics.<sup>[234]</sup> Since  $\text{CeO}_2$  requires  $T > 1500^\circ\text{C}$  and  $p_{\text{O}_2} \approx 1$  mbar to reach moderate degrees of reduction,<sup>[235]</sup> the search for alternative redox materials actually continues. Materials under investigation include doped ceria,<sup>[236–239]</sup> perovskites,<sup>[240–242]</sup> iron oxide,<sup>[243–245]</sup> ferrites,<sup>[246,247]</sup> doped-hercynite<sup>[248–250]</sup> and even materials that undergo a phase change during the process, such as  $\text{ZnO}$ .<sup>[251]</sup>

Besides metal oxide-based redox cycles, the family of sulfur-based thermochemical cycles is one of the most studied (e.g., hybrid sulfur and sulfur-iodine cycles). Such cycles involve the decomposition of the sulfuric acid at high temperature in a corrosive atmosphere. The reactions take place in three steps between  $300^\circ\text{C}$  and  $1000^\circ\text{C}$ .

In order to show the great variety of different cycles and process concepts, a selection of the approaches, currently being investigated, is briefly presented below.

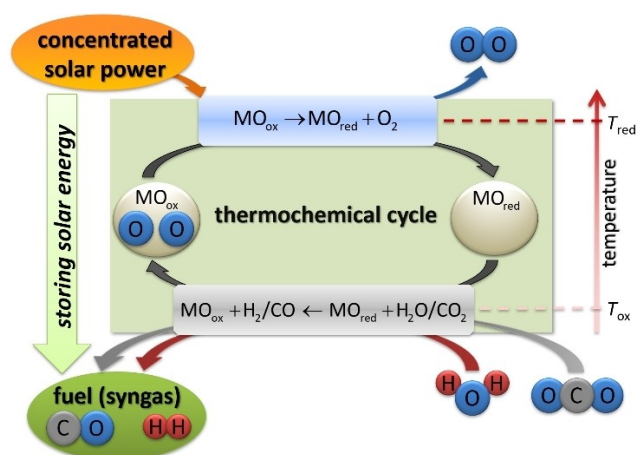


**Figure 10.** Solar driven thermochemical cycle (Figure adapted from Agrafiotis et al.,<sup>[231]</sup> reprint permission by Elsevier).

As part of the SUN-to-LIQUID project,<sup>[252]</sup> an integrated plant was constructed and a receiver-reactor (50 kW scale) was tested in-field.<sup>[253,254]</sup> Co-splitting cycles (water and carbon dioxide ( $\text{CO}_2$ )) for more than 100 days and Fischer–Tropsch synthesis of kerosene from syngas were demonstrated (Figure 11).

The ratio of  $\text{H}_2$  to carbon monoxide ( $\text{CO}$ ) in the product stream can be tailored by the ratio of the educts, which has been demonstrated using a similar type of receiver-reactor with a different solar concentrator.<sup>[256]</sup> Peak conversion rates in the range of 20%–40% have been reported for  $\text{H}_2\text{O}$ <sup>[232]</sup> and  $\text{CO}_2$ ,<sup>[256]</sup> while efficiencies of about 5% have been achieved.<sup>[255]</sup>

The quality of the product stream depends mainly on the purity of the oxidizer and the carrier gases used, such as Argon. Co-splitting has been reported to form small amounts of methane ( $\text{CH}_4$ ).<sup>[257]</sup> Sublimation of the redox material has also been reported, but this is usually removed from the product stream by deposition.<sup>[232]</sup>

In an alternative particle-based implementation, a 5 kW-vacuum receiver-reactor has been integrated into a system with a separate oxidation reactor for the continuous reduction of redox particles.<sup>[258,259]</sup> The system has the advantages of continuous irradiation, easy replacement of the redox material, and temperature control by varying the particle mass flow on a horizontal conveyor.<sup>[260,261]</sup>

Furthermore, the feasibility of solar-powered membrane reactors for  $\text{H}_2$  production or co-production of syngas has been demonstrated.<sup>[262,263]</sup> Membrane reactors can be operated continuously as long as the driving force can be maintained, typically a gradient of chemical potential across the membrane. The greater the chemical potential gradient between the two reactor chambers, the lower the temperature or the higher the conversion efficiency. In comparison to two-step thermochemical water splitting, membrane-based water splitting does not require temperature and/or pressure swing. Most work on membrane-based  $\text{H}_2$  production focuses on oxygen-permeable membranes, such as

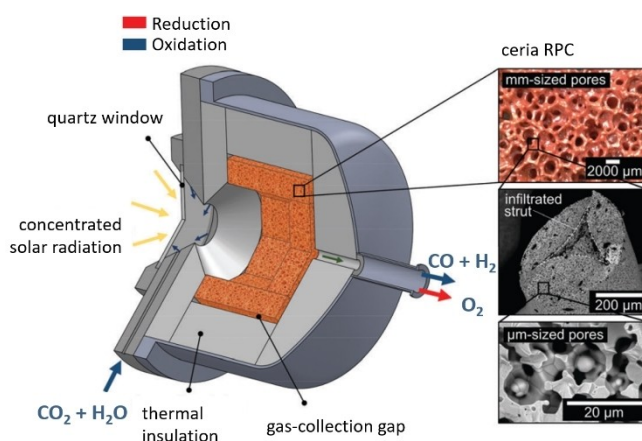


**Figure 11.** Receiver-reactor of the project SUN-to-LIQUID developed by ETHZ (left) and dual-scale ceria RPC (right). Figure adapted from Marxer et al.<sup>[255]</sup> Original image is from a CC BY-NC publication, reprint allowed for non-commercial purposes).

Ceria<sup>[262–264]</sup> or perovskites, e.g., the La–Sr–Fe–Co-oxide system.<sup>[262,264–266]</sup>

An attractive way for pressurizing the produced H<sub>2</sub> using waste heat (e.g., from thermochemical cycles) is by metal hydride compressors (MHC), which operate on the principle of H<sub>2</sub> absorption-desorption as a function of temperature and pressure. MHCs with large compression ratios have several compression stages with different metal hydrides and corresponding absorption and desorption pressures.<sup>[267]</sup> In the European project ATLAS-H<sub>2</sub>, H<sub>2</sub> was compressed from 7 to 220 bar using a MHC operated with hot (80 °C) and cold (10 °C) water.<sup>[268]</sup> In the follow-up ATLAS-MHC project, the exit H<sub>2</sub> pressure was increased over 300 bar.<sup>[269]</sup> MHCs can be economically advantageous over mechanical H<sub>2</sub> compression, especially if waste heat is available.<sup>[267,270]</sup>

### 3.4. Pyrolysis of Hydrocarbons Based on Liquid Metal Reactor Technology

Hydrogen can be produced by thermal decomposition—the so-called pyrolysis process—of hydrocarbon (HC), e.g., methane, which produces also solid carbon (Eq. 4, chapter 3.5). The use of molten metal to crack methane derived from sustainable methods (for instance, biogas) was—to our best knowledge—first proposed by Steinberg.<sup>[271]</sup> This method has significant advantages in heat transfer, but also in carbon capture and removal, especially compared to catalyzed pyrolysis, where the carbon produced as a by-product deactivates the solid catalysts used to boost the reaction to industrially feasible rates. Due to the lower density of carbon compared to liquid metals, the carbon produced floats on the surface of the liquid metal and can be removed by industrial techniques such as skimming. Therefore, the problems associated with reactor clogging or catalyst deactivation due to carbon deposits observed in other processes can be avoided. In addition, obtaining a homogeneous carbon material with a high market value as a by-product of H<sub>2</sub> production is a very attractive option that could significantly influence the price of H<sub>2</sub> produced with liquid metal reactor technology.

For technically relevant CH<sub>4</sub> conversion rates, operation temperatures of about 1000–1200 °C are usually required. However, in order to make the entire process completely CO<sub>2</sub>-free, the necessary reaction heat can be provided by a renewable energy source such as solar thermal energy or electrical energy from photovoltaics (or wind power). For example, solar reactors using concentrated solar energy have already been tested for gas-phase methane pyrolysis<sup>[272]</sup> and could also be coupled with molten metal reactors. They can be heated directly (like reactors at the focal point of parabolic dishes) or indirectly (as in large solar towers with a heat transfer fluid). Molten tin (Sn)-based pyrolysis of methane has been tested using a solar furnace with a parabolic dish,<sup>[273]</sup> while Zheng et al.<sup>[274]</sup> have proposed a system for coupling a solar tower with a liquid metal reactor.

A process for the production of H<sub>2</sub> from methane pyrolysis based on liquid metal technology was demonstrated at KALLA, KIT in Germany.<sup>[275]</sup> Liquid tin was

selected as the working fluid based on several criteria: it is non-toxic and non-explosive, and it has good thermal conductivity, high density compared to carbon, long-term chemical stability, inert behavior towards the reaction gases and carbon,<sup>[276]</sup> attractive cost. The main challenge in the use of liquid tin is the strong corrosion attack at high temperatures on metals, especially steels.<sup>[277]</sup>

Several series of experimental studies on methane conversion in liquid tin were carried out in a bubble column reactor made of stainless steel in combination with quartz glass for the reactor parts that come into contact with the liquid metal. The exemplary experimental setup shown in Figure 12 consists of an approximately 1.3 m high vertical quartz glass tube with an internal diameter of 4 cm, which is filled with liquid tin up to a height of about 1 m in the operating state and is inserted into a stainless-steel tube.<sup>[278]</sup> Methane gas is injected via a single-hole opening at the bottom of the reactor.

In the test campaigns so far, the bubble column has been operated in the range of 900 °C to 1175 °C and slightly at overpressure to compensate for the hydrostatic pressure drop in the reactor. The pressure drop along the column is about 0.7 bar, mainly due to the hydrostatic pressure generated by the liquid tin column. As it can be observed in Figure 13, the maximum H<sub>2</sub> yield of 78 % was achieved at 1175 °C and 50 mln min<sup>-1</sup> of pure methane.<sup>[279]</sup> Only minor amounts (less than 1.5 % in total) of intermediate hydrocarbons (C<sub>2</sub>H<sub>2</sub>, C<sub>2</sub>H<sub>4</sub>, C<sub>2</sub>H<sub>6</sub>) were detected in the product gas.<sup>[277]</sup> Depending on the intended application, further purification process may therefore be required.

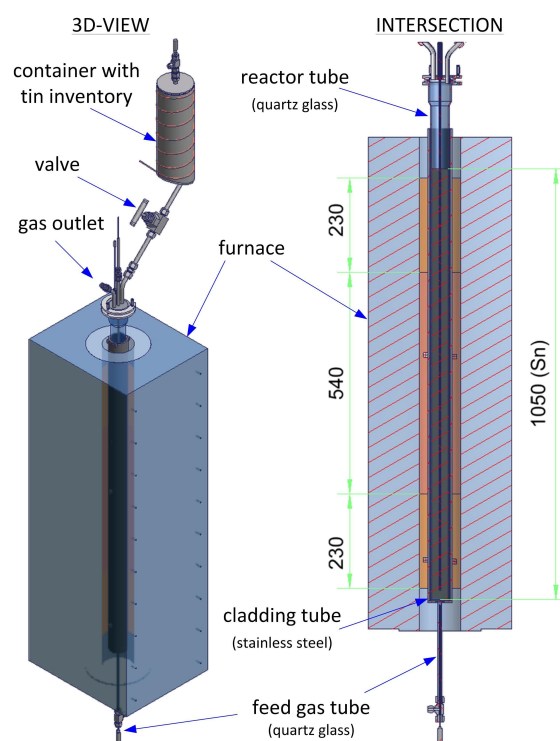


**Figure 12.** Experimental setup of the liquid metal reactor using a combination of quartz glass and stainless steel.<sup>[277]</sup>

It can be noticed that the temperature has a large influence on the resulting methane conversion, while the dependence on the methane volumetric flow rate is moderate. This behavior is the result of a complex interplay between the subsequent passage of the reacting gas through the liquid metal and in the gas phase volumes of the reactor above the liquid tin upper surface.<sup>[279]</sup>

The solid carbon produced was mainly found as a fine powder on the surface of the liquid tin, while only a thin layer of carbon was deposited on the reactor wall. Thus, the tin inventory remained stable and pure with no significant traces of carbon. The preliminary analysis revealed that the produced powder contains carbon in the shape of flakes.

The type of metal used in this technology also has an important influence on the overall performance of the process, which has been studied by several research groups for different liquid metals (Sn, Ga or Ni–Bi and Cu–Bi alloys). In addition to the aforementioned conversion of CH<sub>4</sub> to H<sub>2</sub> with yield of almost 80 % (Figure 13), Msheik et al.<sup>[273]</sup> achieved a conversion of up to 93 % by raising the temperature to 1400 °C in a tubular solar reactor with a liquid tin bath height of 120 mm. Using pure molten Ga, Perez et al.<sup>[280]</sup> achieved a conversion of 91 % at 1119 °C. In addition, Mg was investigated by Wang et al.,<sup>[281]</sup> who reported methane conversion of 30 % at only 700 °C. However, operation at higher temperatures is not possible due to Mg evaporation. As for binary metals, Upham et al.<sup>[282]</sup> tested several molten metal alloys and found that the best performance was achieved with Ni–Bi alloy (Ni<sub>0.27</sub>Bi<sub>0.73</sub>). In this case, methane conversion of 95 % was achieved using a 1.1 m bubble column reactor at 1065 °C. Palmer et al.<sup>[283]</sup> found that Cu<sub>0.45</sub>Bi<sub>0.55</sub> could even surpass the catalytic performance of the Ni–Bi alloy.

In summary, experiments performed by research groups worldwide have demonstrated the technical feasibility of H<sub>2</sub> production from the direct pyrolysis of methane in bubble column reactors filled with various liquid metals such as Sn, Ga<sup>[280]</sup> or Ni–Bi<sup>[282]</sup> and Cu–Bi alloys.<sup>[283]</sup> The application of liquid metal technology avoids the problems associated with reactor clogging due to carbon agglomeration. Further

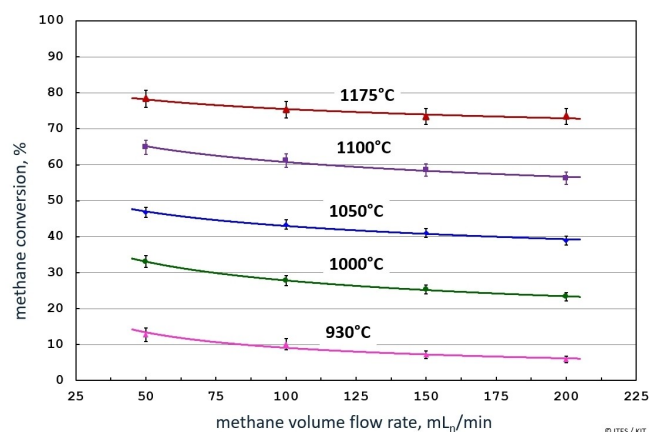


**Figure 13.** Methane conversion vs methane volume flow rate at different temperatures<sup>[279]</sup> (reprint permission by Elsevier).

research work is in progress to find suitable reactor materials for industrial-scale implementation and long-term operation.

### 3.5. Plasma Conversion Technology

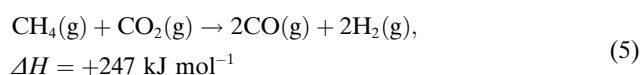
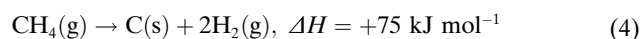
H<sub>2</sub> production driven or assisted by plasma technology is a topic of wide interest, though still with a relatively low readiness (TRL 2–4). It is rooted within a plasma's capability to activate stable molecules such as CH<sub>4</sub>, CO<sub>2</sub>, N<sub>2</sub> or H<sub>2</sub>O by efficiently breaking their chemical bonds and converting them into value-added chemicals. The basis of a plasma process for gas conversion is the delivery of energy to a gas flow for plasma generation. In short, the plasma fulfils two basic functions: it can serve as a heat supplier (several thousand °C can easily be reached, depending on the discharge type), or—if suitable, non-equilibrium conditions can be achieved—as a mean to facilitate reaction pathways entirely inaccessible with purely thermal approaches. In most applications, however, plasma acts as both, which makes its specific function in process chemistry a very complex and actively investigated topic.

Currently, plasma technology is being explored in various Power-to-X (PtX) process chains to provide a technology for decentralized application powered by intermittent energy sources. Plasma processes are being considered for methane-based conversion pathways, both by means of pyrolysis<sup>[284]</sup> and reforming processes.<sup>[285–287]</sup>

Plasma reactors are typically operated at atmospheric pressure and aim to produce pure H<sub>2</sub> or synthesis gas, depending on the process being targeted. The capability for virtually instantaneous operation makes them ideally suited to be paired with green energy sources. Furthermore, the conversion process does not necessarily rely on a catalyst, thus no rare earth materials are utilized during operation. This aspect makes them relatively straightforward to scale-up, primarily via modular and stacking approaches.

The actual coupling of energy into the gas to generate plasma can be done by different concepts in plasma conversion reactors capable to operate at atmospheric pressure. The availability of different types of discharge (Figure 14) allows access to a large parameter space, with different concepts showing potential in various scenarios.<sup>[285,288]</sup>

So far, the use of plasma conversion reactors for H<sub>2</sub> production has been focusing mainly on either methane pyrolysis (MP, Eq. 4) or dry reforming of methane (DRM, Eq. 5):



From the prospective of solar powered green H<sub>2</sub> production, renewable methane is to be considered as a feedstock. Since both CH<sub>4</sub> and CO<sub>2</sub> are the primary emissions from waste gas/biogas processing, the use of

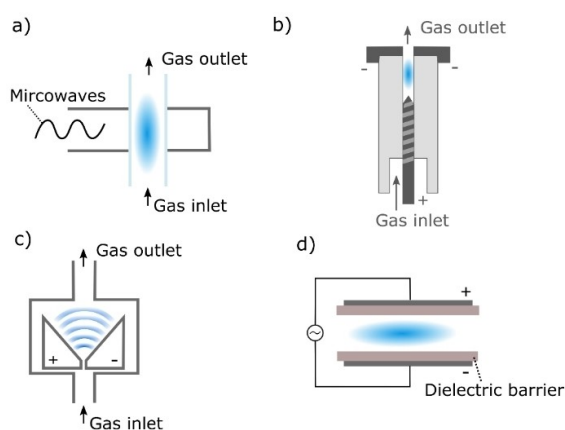


**Figure 14.** Schematic of different plasma discharges: a) microwave (MW) plasma: an electromagnetic wave (typically at frequency of 2.45 GHz or 915 MHz) is used to sustain plasma in a flowing gas mixture within a dielectric tube. Other concepts shown here rely on the generation of the electric field by applying AC high voltage between two electrodes; b) atmospheric plasma gas discharge (APGD): the process gas is fed in a small discharge volume between electrodes which are supplied by DC voltages of several tens of kV; c) gliding arc (GA): the process gas passes high current arc discharges that periodically evolve between the chamfered electrodes; d) dielectric barrier discharge (DBD): one (or in this case both) electrodes are covered by a dielectric that is suppressing high direct currents between the electrodes.

plasma reactors is very attractive. Here, carbon dioxide is used as an oxidizer for  $\text{CH}_4$ , in contrast to the conventional  $\text{H}_2$  production from fossil  $\text{CH}_4$  by steam reforming, which uses water as an oxidizer.<sup>[289]</sup> The transition to  $\text{CO}_2$  as an oxidizer that is consumed instead of being a potential product appears as very appealing for obvious reasons. However, DRM is challenging to achieve with conventional thermal approaches, as it is a highly endothermic process that requires elevated temperatures and thus a catalyst. The latter is in turn very susceptible to deactivation due to soot formation, which drastically limits long-term operation.<sup>[289]</sup> The advantages of plasma conversion technology for DRM and MP now lie in its ability to mitigate many of these limiting factors. For example, achieving thermally inaccessible parameter spaces could reduce or even eliminate the need for heterogeneous catalysis. This depends strongly on the individual properties of the atmospheric plasma (both at high temperatures or at non-equilibrium conditions).<sup>[290–293]</sup>

No additional impurities are introduced by the plasma process, apart from those associated with either the feed-stock gas mixture or a by-product of the process itself (i.e. higher hydrocarbons, oxygen, carbon dioxide), which necessarily require a separation step. As the data collected in recent publications demonstrate,<sup>[285,286,288,294]</sup> plasma conversion reactors based on different discharge types and operating at atmospheric pressure are indeed capable of achieving high  $\text{CH}_4$  and  $\text{CO}_2$  conversion rates at relatively low energy costs. In particular, reactors such as gliding arcs, atmospheric pressure glow discharges and microwave plasmas have demonstrated promising results on a laboratory-scale with regard to the proposed energy efficiency targets for synthesis gas ( $\text{CO} + \text{H}_2$ ) production.<sup>[285]</sup> An increase in the operating pressure to above 1 atm is currently under investigation.<sup>[295]</sup>

On a fundamental level, plasma reactors also have the potential capability to shift the ratio of  $\text{H}_2$  and  $\text{CO}$  as desired products by adapting the gas inflow (i.e.  $\text{CH}_4:\text{CO}_2$  ratio). For example, the ideal molar  $\text{H}_2/\text{CO}$  ratio for most Fischer–Tropsch processes is about two.<sup>[296]</sup> However, even though plasma reactors for DRM do not necessarily rely on catalysts, soot formation can remain a challenge leading to discharge instabilities and choking, especially at  $\text{CH}_4$ -rich conditions.<sup>[289]</sup> Due to the low TRL of all these approaches, several discharge-specific restrictions and limitations still need to be overcome for large-scale application. However, projects targeting the plasma pyrolysis of fossil  $\text{CH}_4$  have demonstrated that plasma conversion technology can achieve a high TRL.<sup>[297]</sup>

Table 2 summarizes the mass yield and the mass yield rate of produced  $\text{H}_2$  (and  $\text{CO}$ ) obtained from specific microwave-driven reactors. However, a direct comparison of conventional (or alternative) processes for  $\text{H}_2$  production with plasma-assisted conversion is difficult, as there is too little data for the latter.

The setups listed in the table are operated both at 2.45 GHz and at 915 MHz, in one case supported by the additional use of catalysts.<sup>[294]</sup> In all cases, the  $\text{CH}_4$ -to- $\text{CO}_2$  gas feed ratio is at (or close to) unity. Reported  $\text{H}_2$  mass yields range from 24 to 59.1  $\text{g}[\text{H}_2]\text{kWh}^{-1}$ , which is in the order of about 60  $\text{g}[\text{H}_2]\text{kWh}^{-1}$  required for economic application<sup>[300]</sup> (corresponding to about 1.5  $\text{kWh m}^{-3}$ ). In all cases, the syngas ratio is close to one, indicating that preferential conditions can be achieved that avoid excessive carbon and water production.<sup>[289]</sup>

**Table 2:** Examples of reported peak performance data for DRM in various microwave plasma reactors at atmospheric pressure.

Discharge type & MW power	Inlet ratio $\text{CH}_4:\text{CO}_2$	$\text{H}_2$ mass yield $[\text{g}[\text{H}_2]\text{kWh}^{-1}]$	$\text{H}_2$ mass yield rate $[\text{g h}^{-1}]$	Product ratio $\text{H}_2:\text{CO}$	$\text{CO}$ yield rate $[\text{kg h}^{-1}]$
2.45 GHz 6 kW <sup>[298]</sup>	50:50	41	240	$\approx 1$	n.a.
2.45 GHz (+ catalyst) 3 kW <sup>[294]</sup>	50:50	59.1	177	$\leq 1$	1.58
915 MHz 4–7.5 kW <sup>[299]</sup>	40:60	24	156	$\approx 1$	n.a.

Plasma conversion technology demonstrates promising results in terms of H<sub>2</sub> and syngas production based on laboratory-scale methane reforming at atmospheric pressure. The main goal for the future is to raise the TRL above the current level. Since the aim of this step is to demonstrate the reliability of the process in relevant environments, the main challenge will be to ensure the desired product selectivity and overall robustness, e.g., avoiding discharge choking due to soot formation when the composition of the feed gas varies.

### 3.6. Electrochemical H<sub>2</sub> Separation and Compression (EHS/EHC)

The emerging need for H<sub>2</sub> production and extraction from low-volume decentralized gas streams, as well as the transportation of H<sub>2</sub>, has opened a niche for the electrochemical extraction/separation and compression (EHS/EHC) of clean, dry H<sub>2</sub>.<sup>[301]</sup> However, the compression of H<sub>2</sub> often presents unique technical challenges not encountered with other process gases such as CH<sub>4</sub> or CO<sub>2</sub>.<sup>[302]</sup> In addition to conventional methods, such as mechanical H<sub>2</sub> compressors,<sup>[303]</sup> or metal hydride and adsorption compressors,<sup>[304]</sup> EHS/EHC can be used to recover H<sub>2</sub> from gas mixtures so that the existing gas transport infrastructure, e.g., for natural gas, can be used.<sup>[305]</sup> Electrochemical pumps have also been used to recover and recirculate unspent H<sub>2</sub> in the fuel cell systems to increase H<sub>2</sub> fuel utilization,<sup>[306,307]</sup> to recover H<sub>2</sub> from reformat products,<sup>[308]</sup> etc.

Such devices typically consist of a solid (ceramic or polymer) electrolyte (membrane) between two electrodes where H<sub>2</sub> oxidation to protons and H<sub>2</sub> reduction (the so called evolution) to H<sub>2</sub> product with certain degree of compression takes place (Eq. 6, 7):



The fact that protonic charges are driven by the applied bias voltage, leading to charge transport, i.e. pumping across the proton conducting membrane (Figure 15), is very important from a practical point of view as it eliminates the need for a pressure gradient across the membrane, which is usually the driving force in passive membranes and Pressure Swing Adsorption (PSA) purification technologies. Furthermore, a high degree of purification can be achieved almost independently of the outlet pressure, while the specific energy consumption of EHC systems decreases with increasing the outlet pressure.<sup>[306,310–313]</sup> EHC also offers safer operation, reduced noise pollution, lower operating and maintenance costs, and less contamination of the H<sub>2</sub> produced<sup>[314]</sup> compared to other compression techniques.

Both the compression and the degree of purity of the resulting H<sub>2</sub> gas depend on several factors. The nature of the proton transport membrane—polymer or ceramic—determines the operating principle and the temperature range of the devices (PEM: T ≤ 100 °C; PCC: T ≥ 400 °C). Membrane

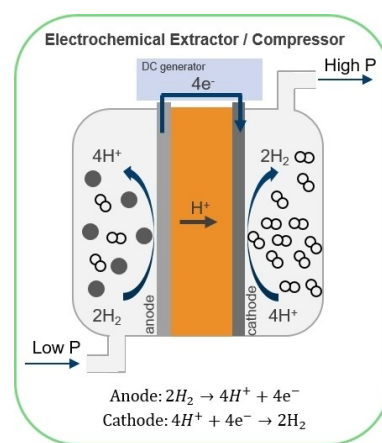


**Figure 15.** Schematic drawing of a H<sub>2</sub> extractor and compressor using a proton conducting membrane (PEM or a solid oxide electrolyte-based cell). H<sub>2</sub> is efficiently extracted from feed streams of low H<sub>2</sub> content and pressurized to 1300 bar (according to the recent SoA in the field of PEM-EHC<sup>[309]</sup>).

materials for EHCs should ideally have a high proton conductivity and high mechanical strength to withstand the pressure difference between the electrodes and H<sub>2</sub> back diffusion. The more mature low-temperature technology can be operated efficiently with pre-purified and pre-compressed gas, while the high-temperature technology offers further advantages that expand its application areas but still requires intensive research effort to gain maturity. In addition, the applied voltage and the H<sub>2</sub> content in the feed stream play an important role for the purification quality and the H<sub>2</sub> recovery factor (HRF): both increase with the H<sub>2</sub> content increase in the feed gas and with the applied voltage.<sup>[312,313,315]</sup>

Presently, PEM<sup>[305,308,310,316–321]</sup> are preferred for low-temperature-EHC, enabling high selectivity and H<sub>2</sub> purity of > 99.9%.<sup>[305,322]</sup> However, as a limitation, they are susceptible to poisoning by CO, NG odorants, CO<sub>2</sub>, S species, etc. Therefore, the combination of H<sub>2</sub> extraction, purification and pre-compression stage with the PEM-EHC final compression stage seem to be very attractive. There are efforts to integrate the purification and compression steps into a single device.<sup>[311]</sup> Although there is a growing number of reports on large-scale pre-commercial EHS/EHC demonstrators, details of such systems are scarce. It has been demonstrated<sup>[323]</sup> that by integrating a PEM-based EHS (25 cm<sup>2</sup>) operating at 35–45 °C into a H<sub>2</sub> storage and recovery system, the H<sub>2</sub> production capacity can be increased. The EHS has not only purified the released H<sub>2</sub> stream, but has also caused higher performance in the dehydrogenation of the liquid organic hydrogen carrier perhydro-dibenzyltoluene (LOHC+ / H18-DBT) by creating a favorable pressure gradient. A compression factor of 12 was demonstrated, resulting in a gain of 6 bar relative to 0.5 bar absolute output pressure. A 120-cell stack was reported<sup>[324]</sup> that achieved a flow rate of about 0.5 lmin<sup>-1</sup> at an outlet pressure of 8.4 bar. The company Giner ELX (now Plug Power) reported a stack that realized 350 bar outlet

pressure. Currently, PEM-based compression of purified H<sub>2</sub> may reach 1300 bar in a single compression stage, starting from 2–10 bar of pre-compressed H<sub>2</sub> (e.g., the technology developed by the company HYET Hydrogen<sup>[309]</sup>). Degradation tests are rare in the literature, however, in the European project MEMPHYS a three-month endurance test was performed on a 5-cell EHP stack, mostly at 200 bar cathode pressure,<sup>[269]</sup> and a recovery rate of 85.3 % was achieved.

PCC can realize EHS up to the highest H<sub>2</sub> purity levels (100% theoretical selectivity) and, in principal, also EHC, which has significant technical implications beyond the fields of fuel cells and electrolysis/co-electrolysis.<sup>[154,325,326]</sup> The design of systems for H<sub>2</sub> extraction, purification from blends and compression in a single step, as well as of highly efficient electrochemical reactors will open the possibility to couple PCC technology to a variety of applications including mobility and chemical/petrochemical processes. To the latter, improved process and system efficiencies can be possibly achieved through thermal integration and chemical equilibrium shift. Important factors on the path to commercialization of such devices are the increased performance and durability of advanced proton conductors, demonstrated directions for industrial application via TEA/LCA aided proof-of-concept (PoC) including system integration concepts and technological upscaling.

### 3.7. Simulation methods

Numerical simulations on various scales (considering dimension, charge carriers, dense/porous transport media in high pressure environments, the effect of impurities, aggregate state of reactants/products, steady state/dynamic mode, etc.) are an important part of research in the field of H<sub>2</sub> production and provide insights for the development and optimization of materials, components, reactors and systems.

The solid electrolyte membranes have the complex task of transferring protons and blocking the crossover of water and O<sub>2</sub> between the electrodes. Their performance is modelled semi-empirically by coupling proton transport with water uptake and diffusive water transport,<sup>[327]</sup> depending on the operating conditions.<sup>[328,329]</sup> Molecular Dynamics (MD) simulations open the possibility of investigating the structure of the solid in both the membrane and the catalyst layer to study permeability and solubility,<sup>[330]</sup> while the impact of impurities in the reactants and products was so far only rarely addressed. Porous layers transport the reactant to the catalyst and the product (mostly in gaseous phase) away. The single and multiphase transport in such layers must be taken into account when optimizing the geometry of the porous layer.<sup>[331–334]</sup> Gas removal from the porous electrodes is a big challenge in water electrolysis.<sup>[331,335,336]</sup> Bipolar plates in electrolyzers and PEC devices also need to be optimized for multiphase flow.<sup>[337]</sup> Computational Fluid Dynamics (CFD)-based methods dealing with multiphase flows apply sharp interface methods (Volume of Fluid, Local Front Reconstruction Method<sup>[338]</sup>) and diffuse interface methods (e.g., the Lattice Boltzmann Method).<sup>[334,339–342]</sup> In

devices for thermochemical water splitting, for example, porous materials are essential to increase the reactive surface area. This complicates mass and heat transport, especially when additional phases describing non-hydrogen gases and limiting the product purity have to be considered. The reactive flow and the radiative heat transport have been modelled in tomographically reconstructed structures.<sup>[332]</sup> In a catalyst layer, e.g., in a photoelectrochemical reactor, where the reactant is in a liquid form and the product in a gaseous form, the multiphase nature of the electrolyte may pose a modelling challenge. The interplay of proton conductivity of the solid, electrical conductivity of the support, gas diffusion in the pores and catalyst utilization is the subject of CFD modelling.<sup>[343]</sup>

In the literature, multiphysics models for single electrolyzers,<sup>[25,344,345]</sup> PEC reactors,<sup>[346–348]</sup> thermochemical water splitting reactors<sup>[349]</sup> and pyrolysis reactors<sup>[350–352]</sup> can be found, usually focusing on a specific reactor design and aim at optimizing the device geometry. 1D–3D simulations consider diffusion, convection, reaction rates, etc., in continuum. These simulations support the reactor's macrostructure design, including optimal dimensions, interaction of the components, transport at variable pressure, performance limits, etc. The device modelling also provides insights about scale-up performance limitations in terms of transport efficiencies or achievable pressures, as well as on the lifetime prediction and the economic optimization of the technology.<sup>[349]</sup> Some components of the devices are complex structures with sophisticated multiphysics behavior and need to be modelled independently to gain a better understanding of the individual processes, as well as of their impact on the performance of the whole reactor.

On the system scale, the interaction of a reactor with the infrastructure can be simulated by replacing the device with an equivalent circuit that resembles the device components or by creating a simplified multiphysics model that includes heat and mass transport at variable pressures, chemical kinetics, radiative transport, semiconductor physics, etc. System-scale modelling is mostly data-driven and describes a particular reactor and its interaction with the infrastructure (energy sources, device interactions within a stack, feed purity, etc.). It helps in life cycle development, evaluation of any performance limits and definition of optimal operation regimes of reactors and electrolyzers.<sup>[306,344,346,353–355]</sup> Attempts are also being made to use machine learning techniques for control the performance of high-temperature PEM electrolyzers.<sup>[356]</sup> A better understanding of the devices can be achieved through more detailed, smaller scale models, which can then potentially be used to build more general and complicated devices with minimal or no fitting parameters.

In summary, great efforts have been invested in the development and application of numerous simulation methods to cover all scales relevant for the optimization of devices for the production of high-quality hydrogen at high pressures. However, thorough studies, covering the entire spectrum and, in particular, the impact of the material and device properties on the purity of the produced H<sub>2</sub>, are, to the best of our knowledge, still lacking. However, it would

be straightforward to systematically add impurities in MD and CFD simulations to understand how to avoid their occurrence or minimize their impact. Optimizing the geometries of membranes, electrodes and even transport devices has been the primary focus of many of the above studies. The next step is to apply the combination of material, process and system-scale simulation to demonstrate how the overall process can be optimized and high-purity H<sub>2</sub> can be achieved under high pressure.

#### 4. Summary and outlook

The production of H<sub>2</sub> from renewable energy sources is one of the most impactful ways to support the establishment of a future carbon neutral and sustainable economy. Amongst others, solar energy in combination with mature or more innovative technologies forms the core of a technology platform for the production of high-purity and compressed green H<sub>2</sub>.

Worldwide, the demand for high-quality H<sub>2</sub> is increasing rapidly, with purity and pressure levels dictated by production routes. To unlock the potential of H<sub>2</sub> as an energy vector with various deployment implications, its quality in terms of purity and degree of compression must meet the intended application requirements. Table 3 provides an overview of the current state of H<sub>2</sub> quality and shows the purity and pressure ranges achieved with the technologies considered in this review paper.

Low-temperature water electrolysis (AWE, PEMWE) has already achieved a high level of technical maturity. Direct coupling with renewable energy production is essential for increasing efficiency and reducing production costs. Continuous operation at low power densities remains problematic as it is the main cause of gas impurities. Since gas contamination is the major factor determining system availability, photovoltaics should be operated at the maximum power point. For optimal operating strategies with high energy efficiency at alternating energy availability, it is essential to analyze the dynamic operating behaviour in more detail. High-temperature technologies for water electrolysis (SOEC, PCEC) combine excellent efficiency through thermal integration of waste heat with superior H<sub>2</sub> purity and operation under moderate pressure. Their

reversible operation makes them an excellent choice for integration into H<sub>2</sub>-based energy storage systems. The attractiveness of SOC technology is reflected in its rapid development in recent years towards higher TRLs.

Devices for photoelectrochemical water splitting offer the advantage of greatly improved thermal management and much lower operating current densities. This greatly reduces the demands on the electrocatalysts. However, no data could be found on the operation of this technology under pressure, while the H<sub>2</sub> purity is considered to be quite similar to that of conventional electrolyzers. The technology is potentially very attractive, however is still in early stage of development, so detailed exploration and proof of concept is required.

Thermochemical water splitting is a technology that can achieve high levels of H<sub>2</sub> purity, depending mostly on possible contaminations in the oxidizer and the carrier gas. Any possible impurities due to sublimation of the redox material are usually removed directly from the product stream by deposition. As far as H<sub>2</sub> compression is concerned, the waste heat from this technology can be coupled with metal hydride compressors (MHC), which are capable of compressing H<sub>2</sub> to over 300 bar in multiple compression stages.

Liquid metal-based pyrolysis of methane is mainly performed at atmospheric pressure, as thermodynamic equilibrium is then favored. Existing studies provide strong evidence that the hydrogen produced has high purity, as the gaseous pyrolysis product contains only small amounts of intermediate species (0.2 mol.% ethane and 1.5 mol.% ethylene<sup>[279]</sup>) and unreacted methane. An economically attractive aspect of H<sub>2</sub> production via pyrolysis of CH<sub>4</sub> is that the carbon obtained as a by-product has various industrial applications. In addition, net negative CO<sub>2</sub> emissions can be achieved when biologically produced CH<sub>4</sub> is used as a feedstock.<sup>[357]</sup>

Plasma conversion technology offers the possibility to operate intermittently (cold start on a second scale), which allows for an ideal adaption to renewable (and inherently unsteady) electrical energy. Currently, the greatest potential of plasma processes is seen mostly in terms of CH<sub>4</sub> reforming processes (methane pyrolysis or dry reforming of methane), where CH<sub>4</sub> from waste gas/biogas plants is used to produce pure H<sub>2</sub> or syngas. Actual plasma reactors operate at atmospheric pressure but do not necessarily rely on the use of catalysts, which is appealing in view of scalability (no rare materials are required). In addition, no impurities apart from those related to either the feedstock gas mixture or a side product of the process itself (i.e. higher hydrocarbons, oxygen, carbon dioxide) occur due to the process. This technology demonstrates promising results at laboratory scale. Raising the TRL of suitable processes is the main future challenge, with a focus on robustness and controlled product selectivity in a relevant environment. This would mean handling the different composition feedstocks, as well as downstream coupling while meeting the respective purity and pressure requirements.

Current research priorities in electrochemical H<sub>2</sub> compression include finding solutions to issues such as high cell

**Table 3:** Purity and pressure ranges achieved with various solar powered technologies. Marked with (\*): purity after cleaning.

Technology	H <sub>2</sub> Purity [%]	Pressure [bar]
AWE	99.8	1–30
AEMWE	> 99.9	1–35 (> 500, low TRL)
PEMWE	> 99.9	30–40 (> 500, low TRL)
SOEC	≥ 99.95*	1–10 (< 30, low TRL)
PCEC	≥ 99.97	1–10 (< 30, prototype targeted)
PEC	≥ 98; > 94 (100 m <sup>2</sup> plant)	1
TCWS	Data not available	> 300 (MHC coupling)
Pyrolysis	≥ 98.5	≤ 1
Plasma	Data not available	1
EHS/EHC	> 99.9	1300

resistance, expensive cell components and relatively short service lifetime. The scale-up of these devices is presently hindered by the inability to operate at high current densities required for greater H<sub>2</sub> pumping rate. At the level of a single cell, it is therefore still essential to reduce membrane resistance to enable operation at high current densities while maintaining mechanical durability. Water management in PEM-EHS/EHC is still not straightforward, as different operating conditions require humidity adjustment. There is still a need to expand the life of the device beyond a few thousand hours by making the Pt (and Ru) catalysts less susceptible to poisoning or finding other alternative materials with comparable or higher H<sub>2</sub> oxidation activity. Finally, despite the low operating and maintenance costs for PEM-EHC, the capital costs, which are presently elevated by the need for special membrane materials and the use of platinum as a catalyst, must be reduced below that of the conventional mechanical compression. Intensive research is being conducted at European level to bring PEM-EHC technology to TRL5 and beyond. In contrast, PCC-EHC technology is still at a relatively early stage of development.

To achieve the goal of leveled costs for H<sub>2</sub> production, the associated capital and operating costs of the deployed technological solutions need to be reduced through increased scalability, efficiency and durability of the devices and plants. Despite the fact that only a few of the solar driven technological pathways have reached sufficient maturity so far, while some of them still display a broad playground for innovation and fundamental research, they all manifest significant potential for meeting the H<sub>2</sub> quality targets. Ultimately, renewably driven technologies for production of H<sub>2</sub> with superior quality are already a compelling alternative to existing solution. Reducing system complexity and increasing installed capacities will pave the way to sustainable and decarbonized future.

### Acknowledgements

The Helmholtz Association of German Research Centers (HGF) and the Federal Ministry of Education and Research (BMBF), Germany are gratefully acknowledged for supporting the development of solar powered technologies for H<sub>2</sub> generation within the frame of the Innovation Pool project “Solar H<sub>2</sub>: Highly Pure and Compressed” and the Helmholtz Research Program “Materials and Technologies for the Energy Transition” (MTET). The publication is also funded by the German Research Foundation (Deutsche Forschungsgemeinschaft DFG)—491111487. Open Access funding enabled and organized by Projekt DEAL.

### Conflict of Interest

The authors declare no conflict of interest.

**Keywords:** H<sub>2</sub> Generation · H<sub>2</sub> Purification and Compression · Methane Pyrolysis · Water Electrolysis · Water Splitting

- [1] <https://hydrogencouncil.com/wp-content/uploads/2017/11/Hydrogen-Scaling-up> Hydrogen-Council 2017.compressed.pdf, **2017**.
- [2] I. Dincer, *Renewable hydrogen production*, Elsevier, Amsterdam, **2022**.
- [3] <https://www.iso.org/standard/69539.html>.
- [4] F. Aupetre, in HYDRAITE 1st OEM Workshop, Ulm, **2018**.
- [5] SAE International, Fuel Standards Committee, S. S. J. Hydrogen Fuel Quality for Fuel Cell Vehicles, Rev March **2020**, <https://doi.org/10.4271/J2719> 202003.
- [6] International Organization for Standardization Hydrogen fuel quality—product specification (ISO Standard No. ISO 14687), **2019**.
- [7] J. M. Ohi, *Fuel Cells: Data, Facts, and Figures* (Eds. D. Stolten, R. C. Samsun, N. Garland), Wiley-VCH, Weinheim, **2016**, pp. 22–29.
- [8] E. Lopez-Fernandez, C. G. Sacedon, J. Gil-Rostra, F. Yubero, A. R. Gonzalez-Elipse, A. de Lucas-Consuegra, *Molecules* **2021**, *26*, 24–50.
- [9] M. David, C. Ocampo-Martinez, R. Sanchez-Pena, *J. Energy Storage* **2019**, *23*, 392–403.
- [10] J. Brauns, T. Turek, *Processes* **2020**, *8*, 248–271.
- [11] O. Ulleberg, *Int. J. Hydrogen Energy* **2003**, *28*, 21–33.
- [12] J. Mougin, *8-Hydrogen production by high-temperature steam electrolysis in Compendium of Hydrogen Energy: Hydrogen Production and Purification* (Eds.: A. B. V. Subramani, T. Nejat Veziroğlu), Woodhead Publishing Series in Energy, **2015**.
- [13] [www.irena.org](http://www.irena.org), **2020**.
- [14] A. Buttler, H. Spliethoff, *Renewable Sustainable Energy Rev.* **2018**, *82*, 2440–2454.
- [15] R. Phillips, C. W. Dunnill, *RSC Adv.* **2016**, *6*, 100643–100651.
- [16] R. Renaud, R. L. Leroy, *Int. J. Hydrogen Energy* **1982**, *7*, 155–166.
- [17] M. R. Kraglund, M. Carmo, G. Schiller, S. A. Ansar, D. Aili, E. Christensen, J. O. Jensen, *Energy Environ. Sci.* **2019**, *12*, 3313–3318.
- [18] M. R. Kraglund, K. J. D. Aili, E. Christensen, Q. Li, J. O. Jensen, *J. Electrochem. Soc.* **2016**, *163*, F3125–F3131.
- [19] J. Hnát, M. Plevova, J. Zitka, M. Paidar, K. Bouzek, *Electrochim. Acta* **2017**, *248*, 547–555.
- [20] J. Hnát, M. Paidar, J. Schauer, J. Zitka, K. Bouzek, *J. Appl. Electrochem.* **2012**, *42*, 545–554.
- [21] O. Omoniyi, T. Bacquart, N. Moore, S. Bartlett, K. Williams, S. Goddard, B. Lipscombe, A. Murugan, D. Jones, *Processes* **2021**, *9*, 1056–1065.
- [22] X. J. Shen, X. Y. Zhang, G. J. Li, T. T. Lie, L. Hong, *Int. J. Energy Res.* **2018**, *42*, 3244–3257.
- [23] D. Pletcher, X. H. Li, *Int. J. Hydrogen Energy* **2011**, *36*, 15089–15104.
- [24] K. Zeng, D. K. Zhang, *Prog. Energy Combust. Sci.* **2010**, *36*, 307–326.
- [25] M. Carmo, D. L. Fritz, J. Mergel, D. Stolten, *Int. J. Hydrogen Energy* **2013**, *38*, 4901–4934.
- [26] A. S. Ansar, A. S. Gago, F. Razmjooei, R. R. Z. Xu, K. A. Friedrich, *Alkaline electrolysis—status and prospects in Hydrogen Production by Water Electrolysis pp. 165–198, in Electrochemical Power Sources: Fundamentals, Systems, and Applications. Hydrogen Production by Water Electrolysis* (Eds.: T. Smolinka, J. Garche), Elsevier, Amsterdam, **2022**.
- [27] D. Y. Xu, M. B. Stevens, M. R. Cosby, S. Z. Oener, A. M. Smith, L. J. Enman, K. E. Ayers, C. B. Capuano, J. N. Renner, N. Danilovic, Y. G. Li, H. Z. Wang, Q. H. Zhang, S. W. Boettcher, *ACS Catal.* **2019**, *9*, 7–15.
- [28] X. Wu, K. Scott, *J. Mater. Chem.* **2011**, *21*, 12344–12351.

- [29] T. Rauscher, C. I. Muller, A. Schmidt, B. Kieback, L. Rontzsch, *Int. J. Hydrogen Energy* **2016**, *41*, 2165–2176.
- [30] T. Rauscher, C. I. Bernacker, U. Muhle, B. Kieback, L. Rontzsch, *Int. J. Hydrogen Energy* **2019**, *44*, 6392–6402.
- [31] Y. S. Park, J. Jeong, Y. Noh, M. J. Jang, J. Lee, K. H. Lee, D. C. Lim, M. H. Seo, W. B. Kim, J. C. Yang, S. M. Choi, *Appl. Catal. B* **2021**, *292*, 120170–120180.
- [32] H. Q. Li, L. Chen, P. F. Jin, H. Lv, H. H. Fu, C. C. Fan, S. L. Peng, G. Wang, J. Hou, F. Yu, Y. L. Shi, *Dalton Trans.* **2020**, *49*, 6587–6595.
- [33] I. Nikolov, R. Darkaoui, E. Zhecheva, R. Stoyanova, N. Dimitrov, T. Vitanov, *J. Electroanal. Chem.* **1997**, *429*, 157–168.
- [34] M. Koj, J. C. Qian, T. Turek, *Int. J. Hydrogen Energy* **2019**, *44*, 29862–29875.
- [35] M. Koj, T. Gimpel, W. Schade, T. Turek, *Int. J. Hydrogen Energy* **2019**, *44*, 12671–12684.
- [36] J. Kim, H. Jung, S. M. Jung, J. Hwang, D. Y. Kim, N. Lee, K. S. Kim, H. Kwon, Y. T. Kim, J. W. Han, J. K. Kim, *J. Am. Chem. Soc.* **2021**, *143*, 1399–1408.
- [37] W. Guo, J. Kim, H. Kim, S. H. Ahn, *Int. J. Hydrogen Energy* **2021**, *46*, 19789–19801.
- [38] R. Gao, D. P. Yan, *Adv. Energy Mater.* **2020**, *10*, 1900954–1900973.
- [39] Y. Cheng, S. P. Jiang, *Prog. Nat. Sci.* **2015**, *25*, 545–553.
- [40] O. Schmidt, A. Gambhir, I. Staffell, A. Hawkes, J. Nelson, S. Few, *Int. J. Hydrogen Energy* **2017**, *42*, 30470–30492.
- [41] S. Marini, P. Salvi, P. Nelli, R. Pesenti, M. Villa, M. Berrettoni, G. Zangari, Y. Kiros, *Electrochim. Acta* **2012**, *82*, 384–391.
- [42] M. Götz, J. Lefebvre, F. Mors, A. M. Koch, F. Graf, S. Bajohr, R. Reimert, T. Kolb, *Renewable Energy* **2016**, *85*, 1371–1390.
- [43] J. Y. Xu, G. Y. Liu, J. L. Li, X. D. Wang, *Electrochim. Acta* **2012**, *59*, 105–112.
- [44] M. A. Laguna-Bercero, *J. Power Sources* **2012**, *203*, 4–16.
- [45] M. Schalenbach, G. Tjarks, M. Carmo, W. Lueke, M. Mueller, D. Stolten, *J. Electrochem. Soc.* **2016**, *163*, F3197–F3208.
- [46] I. V. Pushkareva, A. S. Pushkarev, S. A. Grigoriev, P. Modisha, D. G. Bessarabov, *Int. J. Hydrogen Energy* **2020**, *45*, 26070–26079.
- [47] T. H. Pham, J. S. Olsson, P. Jannasch, *J. Mater. Chem. A* **2018**, *6*, 16537–16547.
- [48] J. S. Olsson, T. H. Pham, P. Jannasch, *Adv. Funct. Mater.* **2018**, *28*, 1702758–1702768.
- [49] Z. C. Liu, S. D. Sajjad, Y. Gao, H. Z. Yang, J. J. Kaczur, R. I. Masel, *Int. J. Hydrogen Energy* **2017**, *42*, 29661–29665.
- [50] G. A. Lindquist, Q. C. Xu, S. Z. Oener, S. W. Boettcher, *Joule* **2020**, *4*, 2549–2561.
- [51] D. Henkensmeier, M. Najibah, C. Harms, J. Zitka, J. Hnat, K. Bouzek, *J. Electrochem. Energy* **2021**, *18*, 024001–024019.
- [52] F. Razmjooei, T. Morawietz, E. Taghizadeh, E. Hadjixenophonos, L. Mues, M. Gerle, B. D. Wood, C. Harms, A. S. Gago, S. A. Ansar, K. A. Friedrich, *Joule* **2021**, *5*, 1776–1799.
- [53] A. Bashkatov, S. S. Hossain, X. G. Yang, G. Mutschke, K. Eckert, *Phys. Rev. Lett.* **2019**, *123*, 214503–214509.
- [54] A. Ursúa, I. S. Martín, E. L. Barrios, P. Sanchis, *Int. J. Hydrogen Energy* **2013**, *38*, 14952–14967.
- [55] M. Schalenbach, W. Lueke, D. Stolten, *J. Electrochem. Soc.* **2016**, *163*, F1480–F1488.
- [56] P. Haug, M. Koj, T. Turek, *Int. J. Hydrogen Energy* **2017**, *42*, 9406–9418.
- [57] M. Sánchez, E. Amores, D. Abad, L. Rodriguez, C. Clemente-Jul, *Int. J. Hydrogen Energy* **2020**, *45*, 3916–3929.
- [58] M. Sánchez, E. Amores, L. Rodriguez, C. Clemente-Jul, *Int. J. Hydrogen Energy* **2018**, *43*, 20332–20345.
- [59] Enapter, <https://handbook.enapter.com/electrolyser/el40/general-information/downloads/Enapter-Datasheet-EL40-EN.pdf>.
- [60] A. Ursúa, P. Sanchis, *Int. J. Hydrogen Energy* **2012**, *37*, 18598–18614.
- [61] K. Onda, T. Kyakuno, K. Hattori, K. Ito, *J. Power Sources* **2004**, *132*, 64–70.
- [62] S. K. Mazloomi, N. Sulaiman, *Renewable Sustainable Energy Rev.* **2012**, *16*, 4257–4263.
- [63] M. N. I. Salehmin, T. Husaini, J. Goh, A. Sulong, *Energy Convers. Manage.* **2022**, *268*, 115985–116010.
- [64] A. Stähler, M. Stähler, F. Scheepers, W. Lehnert, M. Carmo, *J. Electrochem. Soc.* **2022**, *169*, 034522–034531.
- [65] M. Müller, W. Zwaygardt, E. Rauls, M. Hehemann, S. Haas, L. Stolt, H. Janssen, M. Carmo, *Energies* **2019**, *12*, 4150–4164.
- [66] N. A. Kelly, T. L. Gibson, D. B. Ouwkerk, *Int. J. Hydrogen Energy* **2008**, *33*, 2747–2764.
- [67] J. Y. Jia, L. C. Seitz, J. D. Benck, Y. J. Huo, Y. S. Chen, J. W. D. Ng, T. Bilir, J. S. Harris, T. F. Jaramillo, *Nat. Commun.* **2016**, *7*, 13237–13243.
- [68] A. Nakamura, Y. Ota, K. Koike, Y. Hidaka, K. Nishioka, M. Sugiyama, K. Fujii, *Appl. Phys. Express* **2015**, *8*, 107101–107105.
- [69] G. Peharz, F. Dimroth, U. Wittstadt, *Int. J. Hydrogen Energy* **2007**, *32*, 3248–3252.
- [70] L. G. Arriaga, W. Martinez, U. Cano, H. Blud, *Int. J. Hydrogen Energy* **2007**, *32*, 2247–2252.
- [71] D. Shapiro, J. Duffy, M. Kimble, M. Pien, *Sol. Energy* **2005**, *79*, 544–550.
- [72] R. E. Clarke, S. Giddey, F. T. Ciacchi, S. P. S. Badwal, B. Paul, J. Andrews, *Int. J. Hydrogen Energy* **2009**, *34*, 2531–2542.
- [73] O. Atlam, F. Barbir, D. Bezmalinovic, *Int. J. Hydrogen Energy* **2011**, *36*, 7012–7018.
- [74] A. Mraoui, B. Benyoucef, L. Hassaine, *Int. J. Hydrogen Energy* **2018**, *43*, 3441–3450.
- [75] T. N. Duc, K. Goshome, N. Endo, T. Maeda, *Int. J. Hydrogen Energy* **2019**, *44*, 26741–26752.
- [76] B. Paul, *Thesis Direct-coupling of the photovoltaic array and PEM electrolyser in solar-hydrogen systems for remote area power supply*, RMIT University, Melbourne, AUS **2009**.
- [77] T. Maeda, H. Ito, Y. Hasegawa, Z. M. Zhou, M. Ishida, *Int. J. Hydrogen Energy* **2012**, *37*, 4819–4828.
- [78] E. Bilgen, *Energy Convers. Manage.* **2001**, *42*, 1047–1057.
- [79] H. Y. He, Z. G. Lu, X. Q. Guo, C. L. Shi, D. Q. Jia, C. Chen, J. M. Guerrero, *Energies* **2022**, *15*, 1472–1489.
- [80] H. Solmecke, O. Just, D. Hackstein, *Renewable Energy* **2000**, *19*, 333–338.
- [81] R. García-Valverde, C. Miguel, R. Martínez-Bejar, A. Urbina, *Int. J. Hydrogen Energy* **2008**, *33*, 5352–5362.
- [82] A. Garrigós, J. M. Blanes, J. A. Carrasco, J. L. Lizan, R. Beneito, J. A. Molina, *Int. J. Hydrogen Energy* **2010**, *35*, 6123–6130.
- [83] M. Kasper, D. Bortis, J. W. Kolar, *IEEE Trans. Power Electr.* **2014**, *29*, 2511–2526.
- [84] R. García-Valverde, N. Espinosa, A. Urbina, *Int. J. Hydrogen Energy* **2011**, *36*, 10574–10586.
- [85] <https://cordis.europa.eu/project/id/101007165>.
- [86] A. Leonide, Y. Apel, E. Ivers-Tiffée, *ECS Trans.* **2009**, *19*, 81–109.
- [87] J. C. Njodzefon, D. Klotz, A. Kromp, A. Weber, E. Ivers-Tiffée, *J. Electrochem. Soc.* **2013**, *160*, F313–F323.
- [88] A. Kromp, S. Dierickx, A. Leonide, A. Weber, E. Ivers-Tiffée, *J. Electrochem. Soc.* **2012**, *159*, B597–B601.
- [89] H. Timmermann, W. Sawady, D. Campbell, A. Weber, R. Reimert, E. Ivers-Tiffée, *J. Electrochem. Soc.* **2008**, *155*, B356–B359.

- [90] A. Weber, *Fuel Cells* **2021**, *21*, 440–452.
- [91] S. D. Ebbesen, C. Graves, M. Mogensen, *Int. J. Green Energy* **2009**, *6*, 646–660.
- [92] L. Bernadet, C. Moncasi, M. Torrell, A. Tarancon, *Int. J. Hydrogen Energy* **2020**, *45*, 14208–14217.
- [93] E. Ioannidou, S. Neophytides, D. K. Niakolas, *Catalysts* **2019**, *9*, 151–170.
- [94] W. Doenitz, R. Schmidberger, *Int. J. Hydrogen Energy* **1982**, *7*, 321–330.
- [95] W. Doenitz, *Int. J. Hydrogen Energy* **1984**, *9*, 817–821.
- [96] E. Erdle, J. Gross, V. Meyringer, *Utilization of Solar Energy for Hydrogen Production by High Temperature Electrolysis of Steam, in Solar Thermal Energy Utilization* (Ed.: M. Becker), Springer, Berlin, Heidelberg, **1987**.
- [97] W. Doenitz, G. Dietrich, E. Erdle, R. Streicher, *Int. J. Hydrogen Energy* **1988**, *13*, 283–287.
- [98] N. Monnerie, H. von Storch, A. Houaijia, M. Roeb, C. Sattler, *Int. J. Hydrogen Energy* **2017**, *42*, 13498–13509.
- [99] G. Schiller, M. Lang, P. Szabo, N. Monnerie, H. von Storch, J. Reinhold, P. Sundarraaj, *J. Power Sources* **2019**, *416*, 72–78.
- [100] A. Houaijia, S. Breuer, D. Thomey, C. Brosig, J. P. Sack, M. Roeb, C. Sattler, *Energy Proced.* **2014**, *49*, 1960–1969.
- [101] M. Lin, S. Haussener, *Sol. Energy* **2017**, *155*, 1389–1402.
- [102] J. Sanz-Bermejo, J. Munoz-Anton, J. Gonzalez-Aguilar, M. Romero, *Appl. Energy* **2014**, *131*, 238–247.
- [103] A. Ghosh, D. Roy, S. Ghosh, in *IOP Conf. Series*, **2019**, pp. 12112–12116.
- [104] D. Udomsilp, C. Lenser, O. Guillon, N. H. Menzler, *Energy Technol.* **2021**, *9*, 2001062–2001080.
- [105] M. F. Vostakola, B. A. Horri, *Energies* **2021**, *14*, 1280–1333.
- [106] C. Lenser, D. Udomsilp, N. H. Menzler, P. Holtappels, T. Fujisaki, K. Leonard, H. Matsumoto, A. G. Sabato, F. Smeacetto, A. Chrysanthou, S. Molin, *Solid oxide fuel and electrolysis cells, in Adv. Ceram. Energy Convers. Storage* (Ed.: O. Guillon), Elsevier, **2019**, pp. 387–547.
- [107] C. Endler-Schuck, J. Joos, C. Niedrig, A. Weber, E. Ivers-Tiffée, *Solid State Ionics* **2015**, *269*, 67–79.
- [108] A. Mai, V. A. C. Haanappel, S. Uhlenbruck, F. Tietz, D. Stover, *Solid State Ionics* **2005**, *176*, 1341–1350.
- [109] A. Mai, V. A. C. Haanappel, F. Tietz, D. Stover, *Solid State Ionics* **2006**, *177*, 2103–2107.
- [110] N. H. Menzler, F. Tietz, S. Uhlenbruck, H. P. Buchkremer, D. Stover, *J. Mater. Sci.* **2010**, *45*, 3109–3135.
- [111] V. A. Rojek, D. Röhrens, M. Brandner, N. H. Menzler, O. Guillon, A. K. Opitz, M. Bram, *ECS Trans.* **2015**, *68*, 1297–1307.
- [112] J. Joos, M. Ender, I. Rotscholl, N. H. Menzler, E. Ivers-Tiffée, *J. Power Sources* **2014**, *246*, 819–830.
- [113] A. Leonide, V. Sonn, A. Weber, E. Ivers-Tiffée, *J. Electrochem. Soc.* **2008**, *155*, B36–B41.
- [114] D. Klotz, A. Weber, E. Ivers-Tiffée, *Electrochim. Acta* **2017**, *227*, 110–126.
- [115] C. Grosseindemann, N. Russner, S. Dierickx, F. Wankmüller, A. Weber, *J. Electrochem. Soc.* **2021**, *168*, 1375–1393.
- [116] S. B. Beale, M. Andersson, C. Boigues-Muñoz, H. L. Frandsen, Z. J. Lin, S. J. McPhail, M. Ni, B. Sunden, A. Weber, A. Z. Weber, *Prog. Energy Combust. Sci.* **2021**, *85*, 100902–100948.
- [117] N. Russner, S. Dierickx, A. Weber, R. Reimert, E. Ivers-Tiffée, *J. Power Sources* **2020**, *451*, 227552–227558.
- [118] L. G. J. de Haart, S. B. Beale, R. Deja, L. Dittrich, T. Duyster, Q. Fang, S. Foit, S.-M. Groß-Barsnick, U. de Haart, I. Hoven, N. Kruse, C. Lenser, Q. Ma, N. Margaritis, N. H. Menzler, D. Naumenko, M. Nohl, Ro. Peters, D. Sebold, F. Thaler, W. Tiedemann, I. D. Unachukwu, B. Varghese, V. Vibhu, I. C. Vinke, S. Wolf, S. Zhang, J. Zurek, L. Blum, *ECS Trans.* **2021**, *103*, 299–305.
- [119] L. Blum, L. G. J. de Haart, J. Malzbender, N. Margaritis, N. H. Menzler, *Energy Technol.* **2016**, *4*, 939–942.
- [120] H. Geisler, A. Kromp, A. Weber, E. Ivers-Tiffée, *J. Electrochem. Soc.* **2014**, *161*, F778–F788.
- [121] Y. Kobayashi, Y. Ando, H. Kishizawa, K. Tomida, N. Mataka, *Fuel Cell Seminar* **2013**, *51*, 79–86.
- [122] Kyocera, <https://global.kyocera.com/prdct/ecd/sofcl/>.
- [123] G. D. Agnew, R. D. Collins, M. Jorger, S. H. Pyke, R. P. Travis, *Solid Oxide Fuel Cells 10 (Sofc-X), Pts 1 and 2* **2007**, *7*, 105–111.
- [124] A. Mai, F. Fleischhauer, R. Denzler, A. Schuler, *Solid Oxide Fuel Cells 15 (Sofc-Xv)* **2017**, *78*, 97–106.
- [125] Bloom Energy, <https://www.bloomenergy.com/>.
- [126] C. Geipel, K. Hauptmeier, K. Herbrig, F. Mittmann, M. Münch, M. Pötschke, L. Reichel, T. Strohbach, T. Seidel, A. Surrey, C. Walter, *ECS Trans.* **2019**, *91*, 123–132.
- [127] M. C. Williams, S. D. Vora, G. A. Jesionowski, *ECS Trans.* **2020**, *96*, 1–10.
- [128] Elcogen, <https://elcogen.com/products/solid-oxide-fuel-cells/>.
- [129] H. Langnickel, M. Rautanen, M. Gandiglio, M. Santarelli, T. Hakala, M. Acri, J. Kiviahio, *J. Power Source Adv.* **2020**, *2*, 100009–100014.
- [130] R. T. Leah, P. A. Bone, A. Selcuk, M. Rahman, A. Clare, M. Lankin, F. Felix, S. Mukerjee, M. A. Selby, *ECS Trans.* **2019**, *91*, 51–61.
- [131] Sunfire, <https://www.sunfire.de/de/wasserstoff>.
- [132] Q. P. Fang, C. E. Frey, N. H. Menzler, L. Blum, *J. Electrochem. Soc.* **2018**, *165*, F38–F45.
- [133] Y. M. Zhao, H. Q. Xue, X. Jin, B. Xiong, R. H. Liu, Y. Peng, L. Y. Jiang, G. H. Tian, *Int. J. Hydrogen Energy* **2021**, *46*, 38163–38174.
- [134] Z. Liu, B. B. Han, Z. Y. Lu, W. B. Guan, Y. Y. Li, C. J. Song, L. Chen, S. C. Singhal, *Appl. Energy* **2021**, *300*, 117439–117445.
- [135] R. A. George, *J. Power Sources* **2000**, *86*, 134–139.
- [136] C. Walter, K. Schwarze, M. Boltze, K. Herbrig, A. Surrey, *Status of Stack & System Development at Sunfire*, Meet. Abstr. MA2021–2003 2187 in 14th European SOFC & SOE Forum 2020.
- [137] J. Brabandt, O. Posdziech, *Solid Oxide Fuel Cells 15 (Sofc-Xv)* **2017**, *78*, 2987–2995.
- [138] X. Sun, A. D. Bonaccorso, C. Graves, S. D. Ebbesen, S. H. Jensen, A. Hagen, P. Holtappels, P. V. Hendriksen, M. B. Mogensen, *Fuel Cells* **2015**, *15*, 697–702.
- [139] L. Bernadet, G. Gousseau, A. Chatroux, J. Laurencin, F. Mauvy, M. Reytier, *Int. J. Hydrogen Energy* **2015**, *40*, 12918–12928.
- [140] L. Bernadet, J. Laurencin, G. Roux, D. Montinaro, F. Mauvy, M. Reytier, *Electrochim. Acta* **2017**, *253*, 114–127.
- [141] R. Kikuchi, T. Yano, T. Takeguchi, K. Eguchi, *Solid State Ionics* **2004**, *174*, 111–117.
- [142] M. Riedel, M. P. Heddrich, A. Ansar, Q. Fang, L. Blum, K. A. Friedrich, *J. Power Sources* **2020**, *475*, 228682–228694.
- [143] S. H. Jensen, C. Graves, M. Chen, J. B. Hansen, X. Sun, *J. Electrochem. Soc.* **2016**, *163*, F1596–F1604.
- [144] H. Iwahara, T. Esaka, H. Uchida, N. Maeda, *Solid State Ionics* **1981**, *3–4*, 359–363.
- [145] H. Iwahara, *Solid State Ionics* **1996**, *86*, 9–15.
- [146] H. Iwahara, *Solid State Ionics* **1999**, *125*, 271–278.
- [147] I. T. Bello, S. Zhai, S. Y. Zhao, Z. Li, N. Yu, M. Ni, *Int. J. Hydrogen Energy* **2021**, *46*, 37406–37428.
- [148] K. D. Kreuer, *Annu. Rev. Mater. Res.* **2003**, *33*, 333–359.
- [149] P. Berger, F. Mauvy, J.-C. Grenier, N. Sata, A. Magrasó, R. Haugrud, P. R. Slater, *Proton Hydration and Transport Properties in Proton-Conducting Ceramics: Fundamentals and Highlights, in Proton-Conducting Ceramics. From Fundamen-*

- talsto *Applied Research* (Ed.: M. Marrony), Pan Stanford Publishing, Singapore, **2016**, pp. 9–12.
- [150] D. Wickham, A. Hawkes, F. Jalil-Vega, *Appl Energy* **2022**, *305*, 117740–117829.
- [151] M. Marrony, *Proton-Conducting Ceramics. From Fundamentals to Applied Research*, Pan Stanford Publishing, Singapore, **2016**.
- [152] C. Herradon, L. Le, C. Meisel, Y.-D. Kim, C. Cadigan, R. O'Hayre, N. P. Sullivan, *High-Pressure Operation of Proton-Conducting Electrolyzers for High-Temperature Water Splitting*, in ECS Meeting Abstracts, p. 1306.
- [153] C. Duan, J. Huang, N. Sullivan, R. O'Hayre, *Appl Phys Rev* **2020**, *7*, 011314–011354.
- [154] E. Völlestad, R. Strandbakke, M. Tarach, D. Catalan-Martinez, M. L. Fontaine, D. Beeaff, D. R. Clark, J. M. Serra, T. Norby, *Nat. Mater.* **2019**, *18*, 752–762.
- [155] M. Balaguer, Y. J. Sohn, D. Kobertz, S. Kasatkov, A. Fantin, M. Mueller, N. H. Menzler, O. Guillon, M. E. Ivanova, *Solid State Ionics* **2022**, *382*, 115959–115973.
- [156] A. V. Kasyanova, L. R. Tarutina, A. O. Rudenko, J. G. Lyagaeva, D. A. Medvedev, *Russ. Chem. Rev.* **2020**, *89*, 667–692.
- [157] C. Duan, R. Kee, H. Zhu, N. Sullivan, L. Zhu, L. Bian, D. Jennings, R. O'Hayre, *Nat. Energy* **2019**, *4*, 230–240.
- [158] C. Duan, R. Kee, H. Zhu, N. Sullivan, L. Zhu, L. Bian, D. Jennings, R. O'Hayre, *Nat. Energy* **2020**, *5*, 729–729.
- [159] W. Deibert, M. E. Ivanova, Y. Huang, R. Merkle, J. Maier, W. A. Meulenberg, *J. Mater. Chem. A* **2022**, *10*, 2362–2373.
- [160] W. Deibert, M. E. Ivanova, K. Ran, J. Mayer, W. A. Meulenberg, *J. Eur. Ceram. Soc.* **2023**, *43*, 121–129.
- [161] K. Leonard, W. Deibert, M. E. Ivanova, W. A. Meulenberg, T. Ishihara, H. Matsumoto, *Membranes* **2020**, *10*, 339–357.
- [162] K. Leonard, M. E. Ivanova, A. Weber, W. Deibert, W. A. Meulenberg, T. Ishihara, H. Matsumoto, *Solid State Ionics* **2022**, *379*, 115918–115925.
- [163] L. Q. Le, C. H. Hernandez, M. H. Rodriguez, L. Zhu, C. Duan, H. Ding, R. P. O'Hayre, N. P. Sullivan, *J. Power Sources* **2021**, *482*, 228868–228877.
- [164] S. Pirou, Q. J. Wang, P. Khajavi, X. Georgolamprou, S. Ricote, M. Chen, R. Kiebach, *Int. J. Hydrogen Energy* **2022**, *47*, 6745–6754.
- [165] K. Leonard, Y. Okuyama, M. E. Ivanova, W. A. Meulenberg, H. Matsumoto, *ChemElectroChem* **2022**, *9*, e20210166.
- [166] M. Marrony, M. Ancelin, G. Lefevre, J. Dailly, *Solid State Ionics* **2015**, *275*, 97–100.
- [167] K. Leonard, Y. Okuyama, Y. Takamura, Y. S. Lee, K. Miyazaki, M. E. Ivanova, W. A. Meulenberg, H. Matsumoto, *J. Mater. Chem. A* **2018**, *6*, 19113–19124.
- [168] R. J. Braun, A. Dubois, K. Ferguson, C. Duan, C. Karakaya, R. J. Kee, H. Zhu, N. Sullivan, E. Tang, M. Pastula, A. Wood, T. Joia, R. O'Hayre, *ECS Trans.* **2019**, *91*, 997–1008.
- [169] [www.bmbf.de/bmbf/shareddocs/downloads/files/seed-paper-production-annex.pdf](http://www.bmbf.de/bmbf/shareddocs/downloads/files/seed-paper-production-annex.pdf).
- [170] P. Dias, T. Lopes, L. Andrade, A. Mendes, *J. Power Sources* **2014**, *272*, 567–580.
- [171] P. Würfel, U. Würfel, *Physics of solar cells: from basic principles to advanced concepts*, Wiley, Hoboken, **2016**.
- [172] R. van de Krol, B. A. Parkinson, *MRS Energy Sustainability* **2017**, *4*, E13–24.
- [173] S. Kirner, P. Bogdanoff, B. Stannowski, R. van de Krol, B. Rech, R. Schlatmann, *Int. J. Hydrogen Energy* **2016**, *41*, 20823–20831.
- [174] T. J. Jacobsson, V. Fjällström, M. Edoff, T. Edvinsson, *Energy Environ. Sci.* **2014**, *7*, 2056–2070.
- [175] A. C. Nielander, M. R. Shaner, K. M. Papadantonakis, S. A. Francis, N. S. Lewis, *Energy Environ. Sci.* **2015**, *8*, 16–25.
- [176] C. C. L. McCrory, S. Jung, I. M. Ferrer, S. M. Chatman, J. C. Peters, T. F. Jaramillo, *J. Am. Chem. Soc.* **2015**, *137*, 4347–4357.
- [177] H. Wang, L. J. Gao, *Curr. Opin. Electrochem.* **2018**, *7*, 7–14.
- [178] J. H. Yu, F. A. Garcés-Pineda, J. Gonzalez-Cobos, M. Pena-Diaz, C. Rogero, S. Gimenez, M. C. Spadaro, J. Arbiol, S. Barja, J. R. Galan-Mascaros, *Nat. Commun.* **2022**, *13*, 4341–4351.
- [179] W.-H. Cheng, M. H. Richter, M. M. May, J. Ohlmann, D. Lackner, F. Dimroth, T. Hannappel, H. A. Atwater, H.-J. Lewerenz, *ACS Energy Lett.* **2018**, *3*, 1795–1800.
- [180] O. Khaselev, J. A. Turner, *Science* **1998**, *280*, 425–427.
- [181] M. M. May, H.-J. Lewerenz, D. Lackner, F. Dimroth, T. Hannappel, *Nat. Commun.* **2015**, *6*, 8286–8293.
- [182] F. F. Abdi, L. Han, A. H. M. Smets, M. Zeman, B. Dam, R. van de Krol, *Nat. Commun.* **2013**, *4*, 2195–2202.
- [183] J. H. Kim, J.-W. Jang, Y. H. Jo, F. F. Abdi, Y. H. Lee, R. van de Krol, J. S. Lee, *Nat. Commun.* **2016**, *7*, 13380–13389.
- [184] X. Shi, H. Jeong, S. J. Oh, M. Ma, K. Zhang, J. Kwon, I. T. Choi, I. Y. Choi, H. K. Kim, J. K. Kim, *Nat. Commun.* **2016**, *7*, 11943–11949.
- [185] I. Y. Ahmet, Y. Ma, J.-W. Jang, T. Henschel, B. Stannowski, T. Lopes, A. Vilanova, A. Mendes, F. F. Abdi, R. van de Krol, *Sustainable Energy Fuels* **2019**, *3*, 2366–2379.
- [186] W. J. Lee, P. S. Shinde, G. H. Go, E. Ramasamy, *Int. J. Hydrogen Energy* **2011**, *36*, 5262–5270.
- [187] K. R. Tolod, S. Hernández, N. Russo, *Catalysts* **2017**, *7*, 13–36.
- [188] S. Tembhurne, F. Nandjou, S. Haussener, *Nat. Energy* **2019**, *4*, 399–407.
- [189] J. W. Ager, M. R. Shaner, K. A. Walczak, I. D. Sharp, S. Ardo, *Energy Environ. Sci.* **2015**, *8*, 2811–2824.
- [190] J. H. Kim, D. Hansora, P. Sharma, J.-W. Jang, J. S. Lee, *Chem. Soc. Rev.* **2019**, *48*, 1908–1971.
- [191] S. T. I. Holmes-Gentle, C. Suter, S. Haussener, *Int. J. Hydrogen Energy* **2021**, *46*, 10666–10682.
- [192] E. Verlage, S. Hu, R. Liu, R. J. R. Jones, K. Sun, C. X. Xiang, N. S. Lewis, H. A. Atwater, *Energy Environ. Sci.* **2015**, *8*, 3166–3172.
- [193] H. Nishiyama, T. Yamada, M. Nakabayashi, Y. Maehara, M. Yamaguchi, Y. Kuromiya, Y. Nagatsuma, H. Tokudome, S. Akiyama, T. Watanabe, R. Narushima, S. Okunaka, N. Shibata, T. Takata, T. Hisatomi, K. Domen, *Nature* **2021**, *598*, 304–318.
- [194] I. Holmes-Gentle, F. Alherish, F. Bedoya-Lora, K. Hellgardt, *Photoelectrochemical Reaction Engineering for Solar Fuels Production, in Photoelectrochemical Solar Cells* (Ed.: M. S. N. Demirci Sankir), **2018**, pp. 1–41.
- [195] D. A. Vermaas, M. Sassenburg, W. A. Smith, *J. Mater. Chem. A* **2015**, *3*, 19556–19562.
- [196] N. M. Vargas-Barbosa, G. M. Geise, M. A. Hickner, T. E. Mallouk, *ChemSusChem* **2014**, *7*, 3017–3020.
- [197] M. B. McDonald, S. Ardo, N. S. Lewis, M. S. Freund, *ChemSusChem* **2014**, *7*, 3021–3027.
- [198] K. Sun, R. Liu, Y. K. Chen, E. Verlage, N. S. Lewis, C. X. Xiang, *Adv. Energy Mater.* **2016**, *6*, 1600379–1600386.
- [199] S. Chabi, K. M. Papadantonakis, N. S. Lewis, M. S. Freund, *Energy Environ. Sci.* **2017**, *10*, 1320–1338.
- [200] S. Chabi, A. G. Wright, S. Holdcroft, M. S. Freund, *ACS Appl. Mater. Interfaces* **2017**, *9*, 26749–26755.
- [201] C. Özen, K. Obata, P. Bogdanoff, N. Yulianto, H. S. Wasisto, F. F. Abdi, *Sustainable Energy Fuels* **2022**, *6*, 377–385.
- [202] S. Kim, J. Yuk, S. Kim, Y. Song, S. So, K. T. Lee, T. H. Kim, J. H. Ham, *J. Power Sources* **2022**, *524*, 231059–231069.
- [203] I. Holmes-Gentle, F. Hoffmann, C. A. Mesa, K. Hellgardt, *Sustainable Energy Fuels* **2017**, *1*, 1184–1198.
- [204] D. V. Esposito, *Joule* **2017**, *1*, 651–658.

- [205] S. M. H. Hashemi, P. Karnakov, P. Hadikhani, E. Chinello, S. Litvinov, C. Moser, P. Koumoutsakos, D. Psaltis, *Energy Environ. Sci.* **2019**, *12*, 1592–1604.
- [206] K. Obata, A. Mokeddem, F. F. Abdi, *Cell Rep. Phys. Sci.* **2021**, *2*, 100358–100376.
- [207] J. M. Spurgeon, N. S. Lewis, *Energy Environ. Sci.* **2011**, *4*, 2993–2998.
- [208] K. O. Iwu, A. Galeckas, A. Y. Kuznetsov, T. Norby, *Electrochim. Acta* **2013**, *97*, 320–325.
- [209] K. O. Iwu, A. Galeckas, S. Diplas, F. Seland, A. Y. Kuznetsov, T. Norby, *Electrochim. Acta* **2014**, *115*, 66–74.
- [210] K. Q. Xu, A. Chatzidakis, T. Norby, *Photochem. Photobiol. Sci.* **2017**, *16*, 10–16.
- [211] K. Xu, A. Chatzidakis, E. Vøllestad, Q. Ruan, J. Tang, T. Norby, *Int. J. Hydrogen Energy* **2019**, *44*, 587–593.
- [212] T. A. Kistler, N. Danilovic, P. Agbo, *J. Electrochem. Soc.* **2019**, *166*, H656–H661.
- [213] T. A. Kistler, D. Larson, K. Walczak, P. Agbo, I. D. Sharp, A. Z. Weber, N. Danilovic, *J. Electrochem. Soc.* **2019**, *166*, H3020–H3028.
- [214] A. E. Dorfi, A. C. West, D. V. Esposito, *J. Phys. Chem. C* **2017**, *121*, 26587–26597.
- [215] C. W. M. P. Sillen. in *Thesis The effect of gas bubble evolution on the energy efficiency in water electrolysis*, Edited by E. Technische Hogeschool Eindhoven, **1983**.
- [216] B. B. R. Hanke-Rauschenbach, P. Millet, in *Compendium of Hydrogen Energy* (Eds.: A. B. V. Subramani, T. N. Veziroglu), Woodhead Publishing, Oxford, **2015**, pp. 179–224.
- [217] C. A. C. Sequeira, D. M. F. Santos, B. Slijukic, L. Amaral, *Braz. J. Phys.* **2013**, *43*, 199–208.
- [218] D. A. G. Bruggeman, *Ann. Phys.* **1935**, *24*, 665–679.
- [219] I. Holmes-Gentle, F. Bedoya-Lora, F. Alhersh, K. Hellgardt, *J. Phys. Chem. C* **2019**, *123*, 17–28.
- [220] R. L. Curl, *AIChE J.* **1974**, *20*, 184–184.
- [221] M. Schalenbach, T. Hoefner, P. Paciok, M. Carmo, W. Lueke, D. Stolten, *J. Phys. Chem. C* **2015**, *119*, 25145–25155.
- [222] M. Mukaddam, E. Litwiller, I. Pinnau, *Macromolecules* **2016**, *49*, 280–286.
- [223] P. Ravi, J. Noh, *Molecules* **2022**, *27*, 7176–7201.
- [224] A. Vilanova, P. Dias, J. Azevedo, M. Wullenkord, C. Spence, T. Lopes, A. Mendes, *J. Power Sources* **2020**, *454*, 227890–227903.
- [225] A. Landman, H. Dotan, G. E. Shter, M. Wullenkord, A. Houaijia, A. Maljusch, G. S. Grader, A. Rothschild, *Nat. Mater.* **2017**, *16*, 646–651.
- [226] A. Landman, R. Halabi, P. Dias, H. Dotan, A. Mehlmann, G. E. Shter, M. Halabi, O. Naseraldean, A. Mendes, G. S. Grader, A. Rothschild, *Joule* **2020**, *4*, 448–471.
- [227] P. Trinke, B. Benschmann, R. Hanke-Rauschenbach, *Int. J. Hydrogen Energy* **2017**, *42*, 14355–14366.
- [228] P. Trinke, B. Benschmann, R. Hanke-Rauschenbach, *Electrochem. Commun.* **2017**, *82*, 98–102.
- [229] T. Nakamura, *Sol. Energy* **1977**, *19*, 467–475.
- [230] S. Abanades, P. Charvin, G. Flamant, P. Neveu, *Energy* **2006**, *31*, 2805–2822.
- [231] C. Agrafiotis, M. Roeb, C. Sattler, *Renewable Sustainable Energy Rev.* **2015**, *42*, 254–285.
- [232] S. Abanades, G. Flamant, *Sol. Energy* **2006**, *80*, 1611–1623.
- [233] W. C. Chueh, S. M. Haile, *ChemSusChem* **2009**, *2*, 735–739.
- [234] A. de la Calle, A. Bayon, *Int. J. Hydrogen Energy* **2019**, *44*, 1409–1424.
- [235] R. J. Panlener, R. N. Blumenthal, J. E. Garnier, *J. Phys. Chem. Solids* **1975**, *36*, 1213–1222.
- [236] F. Call, M. Roeb, M. Schmücker, H. Bru, D. Curulla-Ferre, C. Sattler, R. Pitz-Paal, *Am. J. Anal. Chem.* **2013**, *4*, 37–45.
- [237] Q. Q. Jiang, G. L. Zhou, Z. X. Jiang, C. Li, *Sol. Energy* **2014**, *99*, 55–66.
- [238] A. Le Gal, S. Abanades, N. Bion, T. Le Mercier, V. Harle, *Energy Fuels* **2013**, *27*, 6068–6078.
- [239] M. Hoes, C. L. Muhich, R. Jacot, G. R. Patzke, A. Steinfeld, *J. Mater. Chem. A* **2017**, *5*, 19476–19484.
- [240] R. J. Carrillo, J. R. Scheffe, *Sol. Energy* **2017**, *156*, 3–20.
- [241] M. Ezbiri, K. M. Allen, M. E. Galvez, R. Michalsky, A. Steinfeld, *ChemSusChem* **2015**, *8*, 1966–1971.
- [242] M. Ezbiri, M. Takacs, D. Theiler, R. Michalsky, A. Steinfeld, *J. Mater. Chem. A* **2017**, *5*, 4172–4182.
- [243] M. Neises, M. Roeb, M. Schmücker, C. Sattler, R. Pitz-Paal, *Int. J. Energy Res.* **2010**, *34*, 651–661.
- [244] P. G. Loutzenhiser, M. E. Galvez, I. Hischer, A. Stamatou, A. Frei, A. Steinfeld, *Energy Fuels* **2009**, *23*, 2832–2839.
- [245] A. Steinfeld, S. Sanders, R. Palumbo, *Sol. Energy* **1999**, *65*, 43–53.
- [246] K. M. Allen, E. N. Coker, N. Auyeung, J. F. Klausner, *Jom-Us* **2013**, *65*, 1670–1681.
- [247] J. R. Scheffe, A. H. McDaniel, M. D. Allendorf, A. W. Weimer, *Energy Environ. Sci.* **2013**, *6*, 963–973.
- [248] C. L. Muhich, B. D. Ehrhart, V. A. Witte, S. L. Miller, E. N. Coker, C. B. Musgrave, A. W. Weimer, *Energy Environ. Sci.* **2015**, *8*, 3687–3699.
- [249] J. R. Scheffe, J. H. Li, A. W. Weimer, *Int. J. Hydrogen Energy* **2010**, *35*, 3333–3340.
- [250] K. J. Warren, J. T. Tran, A. W. Weimer, *Energy Environ. Sci.* **2022**, *15*, 806–821.
- [251] C. L. Muhich, S. Blaser, M. C. Hoes, A. Steinfeld, *Int. J. Hydrogen Energy* **2018**, *43*, 18814–18831.
- [252] www.sun-to-liquid.eu.
- [253] E. Koepf, S. Zoller, S. Luque, M. Thelen, S. Brendelberger, J. Gonzalez-Aguilar, M. Romero, A. Steinfeld, in *AIP Conf. Proc.* **2019**, pp. 180012–180020.
- [254] S. Zoller, E. Koepf, D. Nizamian, M. Stephan, A. Patane, P. Haueter, M. Romero, J. Gonzalez-Aguilar, D. Lieftink, W. E. De, S. Brendelberger, A. Sizmann, A. Steinfeld, *Joule* **2022**, *6*, 1606–1616.
- [255] D. Marxer, P. Furler, M. Takacs, A. Steinfeld, *Energy Environ. Sci.* **2017**, *10*, 1142–1149.
- [256] R. Schächli, D. Rutz, F. Dahler, A. Muroyama, P. Haueter, J. Lilliestam, A. Patt, P. Furler, A. Steinfeld, *Nature* **2022**, *601*, 63–81.
- [257] D. Marxer, P. Furler, J. Scheffe, H. Geerlings, C. Falter, V. Batteiger, A. Sizmann, A. Steinfeld, *Energy Fuels* **2015**, *29*, 3241–3250.
- [258] A. Singh, J. Lapp, J. Grobbel, S. Brendelberger, J. P. Reinhold, L. Olivera, I. Ermanoski, N. P. Siegel, A. McDaniel, M. Roeb, C. Sattler, *Sol. Energy* **2017**, *157*, 365–376.
- [259] A. McDaniel. in *Annual Progress Report of the DOE Hydrogen and Fuel Cells Program*, **2017**.
- [260] I. Ermanoski, J. Grobbel, A. Singh, J. Lapp, S. Brendelberger, M. Roeb, C. Sattler, J. Whaley, A. McDaniel, N. P. Siegel, *AIP Conference Proceedings* **1734**, 120001 (122016), in *Solarpaces 2015: International Conference on Concentrating Solar Power and Chemical Energy Systems*, **2016**.
- [261] I. Ermanoski, A. Orozco, J. Grobbel, *AIP Conf. Proc.* **1850**, 100004 (102017), in *International Conference on Concentrating Solar Power and Chemical Energy Systems (Solarpaces 2016)*, **2017**.
- [262] A. Haeussler, S. Abanades, J. Jouannaux, A. Julbe, *J. Membr. Sci.* **2021**, *634*, 119387–119415.
- [263] M. Tou, J. Jin, Y. Hao, A. Steinfeld, R. Michalsky, *React. Chem. Eng.* **2019**, *4*, 1431–1438.
- [264] U. Balachandran, T. H. Lee, S. E. Dorris, *Int. J. Hydrogen Energy* **2007**, *32*, 451–456.
- [265] A. Evdou, V. Zaspalis, L. Nalbandian, *Fuel* **2010**, *89*, 1265–1273.

- [266] H. Q. Jiang, H. H. Wang, S. Werth, T. Schiestel, J. Caro, *Angew. Chem. Int. Ed.* **2008**, *47*, 9341–9344.
- [267] M. V. Lototsky, V. A. Yartys, B. G. Pollet, R. C. Bowman, *Int. J. Hydrogen Energy* **2014**, *39*, 5818–5851.
- [268] G. Karagiorgis, C. N. Christodoulou, H. von Storch, G. Tzamalidis, K. Deligiannis, D. Hadjipetrou, M. Odysseos, M. Roeb, C. Sattler, *Int. J. Hydrogen Energy* **2017**, *42*, 12364–12374.
- [269] MEMPHYS MEMbrane based Purification of HYdrogen System, D5.5: Report 3-month duration test of prototype sub-size EHP stack, Project Report, **2020**.
- [270] E. Stamatakis, E. Zoulias, G. Tzamalidis, Z. Massina, V. Analytis, C. Christodoulou, A. Stubos, *Renewable Energy* **2018**, *127*, 850–862.
- [271] M. Steinberg, *Int. J. Hydrogen Energy* **1999**, *24*, 771–777.
- [272] M. Msheik, S. Rodat, S. Abanades, *Energies* **2021**, *14*, 3107–3142.
- [273] M. Msheik, S. Rodat, S. Abanades, *Energy* **2022**, *260*, 124943–124977.
- [274] Z. J. Zheng, Y. Xu, *Energy Convers. Manage.* **2018**, *157*, 562–574.
- [275] A. Abánades, R. K. Rathnam, T. Geissler, A. Heinzel, K. Mehravaran, G. Muller, M. Plevan, C. Rubbia, D. Salmieri, L. Stoppel, S. Stuckrad, A. Weisenburger, H. Wenninger, T. Wetzel, *Int. J. Hydrogen Energy* **2016**, *41*, 8159–8167.
- [276] J. Pacio, T. Wetzel, *Sol. Energy* **2013**, *93*, 11–22.
- [277] L. Stoppel, T. Fehling, T. Geissler, E. Baake, T. Wetzel, *IOP Conf. Ser.: Mater. Sci. Eng.* **2017**, *228*, 012016–012031.
- [278] M. Plevan, T. Geissler, A. Abanades, K. Mehravaran, R. K. Rathnam, C. Rubbia, D. Salmieri, L. Stoppel, S. Stuckrad, T. Wetzel, *Int. J. Hydrogen Energy* **2015**, *40*, 8020–8033.
- [279] T. Geissler, A. Abanades, A. Heinzel, K. Mehravaran, G. Muller, R. K. Rathnam, C. Rubbia, D. Salmieri, L. Stoppel, S. Stuckrad, A. Weisenburger, H. Wenninger, T. Wetzel, *Chem. Eng. J.* **2016**, *299*, 192–200.
- [280] B. J. Leal Pérez, J. A. M. Jimenez, R. Bhardwaj, E. Goetheer, M. V. Annaland, F. Gallucci, *Int. J. Hydrogen Energy* **2021**, *46*, 4917–4935.
- [281] K. Wang, W. S. Li, X. P. Zhou, *J. Mol. Catal. A* **2008**, *283*, 153–157.
- [282] D. C. Upham, V. Agarwal, A. Khechfe, Z. R. Snodgrass, M. J. Gordon, H. Metiu, E. W. McFarland, *Science* **2017**, *358*, 917–920.
- [283] C. Palmer, M. Tarazkar, H. H. Kristoffersen, J. Gelinas, M. J. Gordon, E. W. McFarland, H. Metiu, *ACS Catal.* **2019**, *9*, 8337–8345.
- [284] M. Jasinski, D. Czynkowski, B. Hrycak, M. Dors, J. Mizeraczyk, *Int. J. Hydrogen Energy* **2013**, *38*, 11473–11483.
- [285] R. Snoeckx, A. Bogaerts, *Chem. Soc. Rev.* **2017**, *46*, 5805–5863.
- [286] X. M. Tao, M. G. Bai, X. A. Li, H. L. Long, S. Y. Shang, Y. X. Yin, X. Y. Dai, *Prog. Energy Combust. Sci.* **2011**, *37*, 113–124.
- [287] R. S. Abiev, D. A. Sladkovskiy, K. V. Semikin, D. Y. Murzin, E. V. Rebrov, *Catalysts* **2020**, *10*, 1358–1397.
- [288] B. Wanten, S. Maerivoet, C. Vantomme, J. Slaets, G. Trenchev, A. Bogaerts, *J. CO<sub>2</sub> Util.* **2022**, *56*, 101869–101880.
- [289] J. M. Lavoie, *Front. Chem.* **2014**, *2*, 81–98.
- [290] N. Sanchez-Bastardo, R. Schlogl, H. Ruland, *Chem. Ing. Tech.* **2020**, *92*, 1596–1609.
- [291] S. Rodat, S. Abanades, G. Flamant, *Sol. Energy* **2011**, *85*, 645–652.
- [292] N. Britun, T. Silva, G. X. Chen, T. Godfroid, J. van der Mullen, R. Snyders, *J. Phys. D* **2018**, *51*, 144002–144016.
- [293] F. A. D'Isa, E. A. D. Carbone, A. Hecimovic, U. Fantz, *Plasma Sources Sci. Technol.* **2020**, *29*, 105009–105028.
- [294] S. M. Chun, D. H. Shin, S. H. Ma, G. W. Yang, Y. C. Hong, *Catalysts* **2019**, *9*, 292–310.
- [295] R. H. Rad, V. Brüser, M. Schiorlin, R. Brandenburg, *Chem. Eng. J.* **2023**, *456*, 141072–141098.
- [296] M. Ostadi, E. Rytter, M. Hillestad, *Biomass Bioenergy* **2019**, *127*, 105282–105291.
- [297] S. Schneider, S. Bajohr, F. Graf, T. Kolb, *ChemBioEng Rev.* **2020**, *7*, 150–158.
- [298] S. M. Chun, Y. C. Hong, D. H. Choi, *J. CO<sub>2</sub> Util.* **2017**, *19*, 221–229.
- [299] B. Hrycak, D. Czynkowski, M. Jasinski, M. Dors, J. Mizeraczyk, *Plasma Chem. Plasma Process.* **2019**, *39*, 695–711.
- [300] K. U. J. Mizeraczyk, M. Jasinski, M. Dors, *Int. J. Plasma Environ. Sci. Technol.* **2014**, *8*, 89–97.
- [301] M. Rhandi, M. Tregaro, F. Druart, J. Deseure, M. Chatenet, *Chin. J. Catal.* **2020**, *41*, 756–769.
- [302] L. S. Mark Barton, J. Stahley, A. Talakar, *Hydrocarbon Engineering* **2021**, <https://assets.siemens-energy.com/siemens/assets/api/uuid:d985fced-fb987e-4881-a4881b4889-4887cd4886d4887eac4863/se-he-august2021-challenges-hydrogen-compression-article.pdf>.
- [303] <https://www.neuman-esser.de>.
- [304] G. Sdanghi, G. Maranzana, A. Celzard, V. Fierro, *Renewable Sustainable Energy Rev.* **2019**, *102*, 150–170.
- [305] L. Vermaak, H. W. J. P. Neomagus, D. G. Bessarabov, *Membranes* **2021**, *11*, 11–35.
- [306] W. Wiebe, T. von Unwerth, S. Schmitz, *Fuel Cells* **2020**, *20*, 362–369.
- [307] F. Barbir, H. Gorgun, *J. Appl. Electrochem.* **2007**, *37*, 359–365.
- [308] D. B. G. Venugopalan, E. Andrews, L. Briceno-Mena, J. Romagnoli, J. Flake, C. G. Arges, *ACS Energy Lett.* **2022**, *7*, 1322–1329.
- [309] <https://hyethydrogen.com>.
- [310] K. Murdoch, R. Blanchard, S. Mukerjee, T. Stracensky, M. Sharma, R. Pavlicek, E. DeCastro, Z. Greenwood, *Closed Loop Hydrogen Recovery Enabled by Electrochemical Hydrogen Separation*, in *49th International Conference on Environmental Systems*, **2019**.
- [311] L. Schorer, S. Schmitz, A. Weber, *Int. J. Hydrogen Energy* **2019**, *44*, 12708–12714.
- [312] M. Nordio, F. Rizzi, G. Manzolini, M. Mulder, L. Raymakers, M. V. Annaland, F. Gallucci, *Chem. Eng. J.* **2019**, *369*, 432–442.
- [313] J. X. Zou, N. Han, J. Y. Yan, Q. Feng, Y. J. Wang, Z. L. Zhao, J. T. Fan, L. Zeng, H. Li, H. J. Wang, *Electrochem. Energy Rev.* **2020**, *3*, 690–729.
- [314] M. Suermann, T. Kiupel, T. J. Schmidt, F. N. Büchi, *J. Electrochem. Soc.* **2017**, *164*, F1187–F1195.
- [315] G. Sdanghi, G. Maranzana, A. Celzard, V. Fierro, *Energies* **2020**, *13*, 3145–3172.
- [316] I. T. Cousins, G. Goldenman, D. Herzke, R. Lohmann, M. Miller, C. A. Ng, S. Patton, M. Scheringer, X. Trier, L. Vierke, Z. Y. Wang, J. C. DeWitt, *Environ. Sci. Proc. Imp.* **2019**, *21*, 1803–1815.
- [317] G. H. X. Wu, L. Yu, X. Li, *ACS Sustainable Chem. Eng.* **2014**, *2*, 75–79.
- [318] Advent Technologies, <https://www.advent.energy/products-high-temperature-meas/>.
- [319] S. S. Araya, S. Thomas, A. Lotric, S. L. Sahlin, V. Liso, S. J. Andreasen, *Energies* **2021**, *14*, 2994–3012.
- [320] F. Huang, A. T. Pingitore, B. C. Benicewicz, *J. Electrochem. Soc.* **2020**, *167*, 063504–063515.
- [321] G. Eisman, D. Share, C. Carlstrom, *Process intensification of hydrogen unit operations using an electrochemical device*, **2012**.
- [322] B. L. Kee, D. Curran, H. Y. Zhu, R. J. Braun, S. C. DeCaluwe, R. J. Kee, S. Ricote, *Membranes* **2019**, *9*, 77–91.

- [323] S. Mrusek, P. Preuster, K. Muller, A. Bosmann, P. Wasserscheid, *Int. J. Hydrogen Energy* **2021**, *46*, 15624–15634.
- [324] B. Shen, S. Fackler, B. Bamdad, *Experimental Study to Characterize Performance of a Prototype Electrochemical Compressor*, Paper 2524 in *International Compressor Engineering Conference*, **2018**.
- [325] S. Choi, C. J. Kucharczyk, Y. G. Liang, X. H. Zhang, I. Takeuchi, H. I. Ji, S. M. Haile, *Nat. Energy* **2018**, *3*, 202–210.
- [326] S. R. Wang, X. Hao, W. T. Zhan, *Int. J. Hydrogen Energy* **2017**, *42*, 29881–29887.
- [327] E. J. F. Dickinson, G. Smith, *Membranes* **2020**, *10*, 310–363.
- [328] K. D. P. M. Bampaou, A. I. Papadopoulos, P. Seferlis, S. Voutetakis, *Chem. Eng. Trans.* **2018**, *70*, 1213–1218.
- [329] G. Sdanghi, J. Dillet, S. Didierjean, V. Fierro, G. Maranzana, *Operating heterogeneities in a PEM Electrochemical Hydrogen Compressor*, hal-02186747 in *8th International Conference on Fundamentals and Development of Fuel Cells*, **2019**.
- [330] R. Jinnouchi, K. Kudo, N. Kitano, Y. Morimoto, *Electrochim. Acta* **2016**, *188*, 767–776.
- [331] F. Arbabi, H. Montazeri, R. Abouatallah, R. Wang, A. Bazylak, *J. Electrochem. Soc.* **2016**, *163*, F3062–F3069.
- [332] A. Akolkar, J. Petrasch, *Transport Porous Med.* **2012**, *95*, 535–550.
- [333] W. Wu, F. M. Jiang, *Int. J. Hydrogen Energy* **2014**, *39*, 15894–15906.
- [334] P. Sarkezi-Selsky, H. Schmies, A. Kube, A. Latz, T. Jahnke, *J. Power Sources* **2022**, *535*, 231381–231395.
- [335] T. Kadyk, D. Bruce, M. Eikerling, *Sci. Rep.* **2016**, *6*, 38780–38794.
- [336] C. Lee, J. K. Lee, B. Zhao, K. F. Fahy, J. M. LaManna, E. Baltic, D. S. Hussey, D. L. Jacobson, V. P. Schulz, A. Bazylak, *J. Power Sources* **2020**, *446*, 227312–227348.
- [337] K. H. Rho, Y. Na, T. Ha, D. K. Kim, *Membranes* **2020**, *10*, 441–456.
- [338] A. H. Rajkotwala, A. Panda, E. A. J. F. Peters, M. W. Baltussen, C. W. M. van der Geld, J. G. M. Kuerten, J. A. M. Kuipers, *Int. J. Multiphase Flow* **2019**, *120*, 103093–103108.
- [339] H. H. Liu, Q. J. Kang, C. R. Leonardi, S. Schmieschek, A. Narvaez, B. D. Jones, J. R. Williams, A. J. Valocchi, J. Harting, *Comput. Geosci.* **2016**, *20*, 777–805.
- [340] N. Kulyk, D. Berger, A. S. Smith, J. Harting, *Comput. Phys. Commun.* **2020**, *256*, 107443–107453.
- [341] Y. L. Wang, H. K. Xu, Z. Zhang, H. Li, X. D. Wang, *Appl. Energy* **2022**, *320*, 119248–119262.
- [342] J. L. Yu, D. Froning, U. Reimer, W. Lehnert, *J. Power Sources* **2019**, *438*, 226975–226987.
- [343] C. V. Pham, D. Escalera-Lopez, K. Mayrhofer, S. Cherevko, S. Thiele, *Adv. Energy Mater.* **2021**, *11*, 2101998–2102023.
- [344] F. Marangio, M. Santarelli, M. Cali, *Int. J. Hydrogen Energy* **2009**, *34*, 1143–1158.
- [345] M. Persson, D. Mignard, D. Hogg, *Int. J. Hydrogen Energy* **2020**, *45*, 31396–31409.
- [346] M. A. Modestino, S. Haussener, *Annu. Rev. Chem. Biomol. Eng.* **2015**, *6*, 13–34.
- [347] S. Haussener, C. X. Xiang, J. M. Spurgeon, S. Ardo, N. S. Lewis, A. Z. Weber, *Energy Environ. Sci.* **2012**, *5*, 9922–9935.
- [348] C. X. Xiang, A. Z. Weber, S. Ardo, A. Berger, Y. K. Chen, R. Coridan, K. T. Fountaine, S. Haussener, S. Hu, R. Liu, N. S. Lewis, M. A. Modestino, M. M. Shaner, M. R. Singh, J. C. Stevens, K. Sun, K. Walczak, *Angew. Chem. Int. Ed.* **2016**, *55*, 12974–12988.
- [349] M. Roeb, M. Neises, J. P. Sack, P. Rietbrock, N. Monnerie, J. Dersch, M. Schmitz, C. Sattler, *Int. J. Hydrogen Energy* **2009**, *34*, 4537–4545.
- [350] F. Angikath, F. Abdulrahman, M. Khandavilli, X. Y. Zhang, S. M. Sarathy, *Energy Fuels* **2021**, *35*, 14597–14609.
- [351] T. C. Farmer, E. W. McFarland, M. F. Doherty, *Int. J. Hydrogen Energy* **2019**, *44*, 14721–14731.
- [352] L. J. J. Catalan, E. Rezaei, *Int. J. Hydrogen Energy* **2020**, *45*, 2486–2503.
- [353] A. Hernández-Gómez, V. Ramirez, D. Guilbert, *Int. J. Hydrogen Energy* **2020**, *45*, 14625–14639.
- [354] V. M. Wheeler, R. Bader, P. B. Kreider, M. Hangi, S. Haussener, W. Lipinski, *Sol. Energy* **2017**, *156*, 149–168.
- [355] L. Zachert, M. Suermann, B. Bensmann, R. Hanke-Rauschenbach, *J. Electrochem. Soc.* **2021**, *168*, 014504–014519.
- [356] D. Q. Zhao, Q. J. He, J. Yu, M. T. Guo, J. Fu, X. Li, M. Ni, *Int. J. Hydrogen Energy* **2022**, *47*, 8687–8699.
- [357] C. Palmer, D. C. Upham, S. Smart, M. J. Gordon, H. Metiu, E. W. McFarland, *Nat. Catal.* **2020**, *3*, 83–89.

Manuscript received: December 20, 2022

Accepted manuscript online: January 13, 2023

Version of record online: May 9, 2023